# VANADIUM DIOXIDE-BASED MATERIALS FOR POTENTIAL THERMAL SWITCHING APPLICATIONS

By

Minyoung Jeong

#### A THESIS

Submitted to
Michigan State University
in partial fulfillment of the requirements
for the degree of

Materials Science and Engineering – Master of Science

2013

#### **ABSTRACT**

## VANADIUM DIOXIDE-BASED MATERIALS FOR POTENTIAL THERMAL SWITCHING APPLICATIONS

By

## Minyoung Jeong

One of the materials able to exhibit a transition from insulators to metals (IMT materials) is vanadium dioxide (VO<sub>2</sub>). Through IMT, VO<sub>2</sub> shows a drop of resistivity of five orders of magnitude at a picosecond timescale. In this work, the feasibility of using VO<sub>2</sub> as an efficient thermal switching device is discussed.

Several synthesis methods (sol-gel, hot press and spark plasma sintering) were attempted to obtain VO<sub>2</sub> sample in pellet form. From the X-ray diffraction results, it was found that spark plasma sintering (SPS) yielded the highest phase purity. Several sintering parameters such as temperature or sintering time were tested to determine the optimal sintering conditions.

For better thermal switching behavior, high-energy ball milling was used to reduce lattice thermal conductivity ( $k_{lat}$ .) in the insulator phase. Ball-milling time was varied from 30 minutes to 2 hours. It was found that with increasing milling time, the  $k_{lat}$  was reduced. Thus, it was demonstrated that thermal switching behavior was most efficient with 2 hour-milling.

To improve electronic thermal conductivity ( $k_{elec}$ .) in the metallic state, nano-sized copper particles were added to the VO<sub>2</sub> system with a subtle amount variation ranging from 3at % to 5 at%. Results show that a composite with 5 at% Cu (copper) addition exhibited the largest increase in thermal conductivity (k) in the metallic state.

#### **ACKNOWLEDGEMENTS**

It is by far my great honor to present my work conducted at Michigan State University for two years. Things I have learned in those two years not only include the knowledge and research skills required to be a professional engineer, but also include what it takes to live a successful life, for example, self-control, passion and so on. For this reason, I feel very grateful for all the support that my advisor, Dr.Morelli, gave to me through the past years. From him, I learned many lessons how to be a committed engineer while at the same time, how to be a mature and intellectual adult.

I deeply appreciate comments and encouragements my committee professors

(Dr.Sakamoto, Dr.Nicholas and Dr.Hogan) gave on my work. I also want to thank my lab-mates

(Xu Lu, Stephen Boona, Gloria Lehr and Vijay Ponnambalam) for their eagerness to help and for their friendliness.

Finally, I want to give many thanks to all the members at my church, Lansing Korean United Methodist Church, for their great support and sincere prayers for me. Pastor Cho and Mrs.Cho, without you, this thesis would have been an impossible task for me.

I always love my family, and it is definitely the most thankful and biggest gift for me to be one of them.

## **TABLE OF CONTENTS**

LIST O	F TABLES	vi
LIST O	F FIGURES	vii
СНАРТ	TER 1. INTRODUCTION	1
СНАРТ	TER 2. BACKGROUND AND MOTIVATION	3
2.1	Band theory of solids	3
2.2	Insulator to Metal Transition (IMT) phenomena	4
2.3	Basic IMT mechanisms	8
2.4	Applications of IMT	12
2.5	Thermal switching	
2.6	Vanadium dioxide for thermal switching	
2.7	Summary	24
СНАРТ	TER 3. METHODS AND PROCEDURES	25
3.1	Synthesizing pure VO <sub>2</sub>	25
i)	Materials	25
i)	Procedures	26
3.2	Synthesizing VO <sub>2</sub> -Cu Composites	31
i)	Materials	31
ii)	Procedures	31
3.3	Transport Property Measurements	32
СНАРТ	TER 4. RESULTS AND DISCUSSION	35
4.1	VO <sub>2</sub> Synthesis	35
i)	Hot Pressed Specimens	35
ii)	Spark Plasma Sintered Specimens	38
iii)	Sol-Gel Technique Specimens	44
4.2	Modifications on VO <sub>2</sub> specimens	45
i)	High-energy ball-milling	
ii)	VO <sub>2</sub> -Cu Composites	49
СНАРТ	TER 5. Conclusions	57
СНАРТ	TER 6. FUTURE RESEARCH CONSIDERATIONS	58
RIRI IC	OGRAPHY	60
אשעוע	$J \cup I \cup $	00

## LIST OF TABLES

Table 3.1 The temperature and time variations in SPS for pure VO <sub>2</sub> synthesis	. 29
Table 3.2 The time-variations in ball-milling and sintering parameters for each sample	. 31
Table 3.3 The compositions and amounts used to synthesize VO <sub>2</sub> -Cu composites	. 32
Table 4.1 The relative densities under different SPS conditions	. 39
Table 4.2 The $\kappa$ changes in a 300K-350K region for different VO <sub>2</sub> -Cu composites	. 55

## LIST OF FIGURES

<b>Figure 2.1</b> Illustration of atomic energy levels splitting into energy bands when atoms are brought together to form a molecule [5] [6]
<b>Figure 2.2</b> The observation of a sudden drop in resistivity in a 100 nm-thick VO <sub>2</sub> thin-film through IMT. [7]
<b>Figure 2.3</b> The VO <sub>2</sub> 's reflection property change in light reflectivity measured for a 100nm VO <sub>2</sub> thin-film sample. [7]
<b>Figure 2.4</b> The light transmission percentages change for different wavelengths as a VO <sub>2</sub> thin-film sample deposited onto a sapphire substrate undergoes a transition at 67°C [8]
<b>Figure 2.5</b> The formation of upper Hubbard band (UHB) and lower Hubbard band (LHB) due to electron correlation [11]
<b>Figure 2.6</b> The 1-D atomic configuration of normal lattice and the distorted lattice, and the corresponding electronic band structures of normal and distorted lattice respectively. [11] 10 Figure 2.7 The lattice potential and corresponding density of states for (top) perfect crystal 11
<b>Figure 2.8</b> I-V curves of thin film VO <sub>2</sub> devices. The W indicates thin-film mesa width. (40, 60, 80 and 100 μm were used) The inset shows the critical current fitted for different W values. [14]
<b>Figure 2.9</b> A cell phone (a) without and (b) with a VO <sub>2</sub> -based device in a cell phone to prevent battery explosion. [33]
<b>Figure 2.10</b> A thermal switch controlling the temperature of electronics device in a spacecraft [17]
<b>Figure 2.11</b> The unit-cell structure of VO <sub>2</sub> (left) after and (right) before transition. "MST" stands for metal to semiconductor transition. [20]
<b>Figure 2.12</b> A VO <sub>2</sub> thermal conductivity, $k$ , curve in (a) thin-film (b) bulk form. In (a), the red triangle-line indicates the values obtained when heating and the black one from cooling. [21,22]
<b>Figure 2.13</b> A VO <sub>2</sub> thin-film thermal conductivity curve. The numbers indicate the film thickness. [23]

Figure 2.14 A descriptive schematic of an intended VO <sub>2</sub> -copper composite. The blue dots
indicate copper particle inclusions inside the VO <sub>2</sub> matrix
<b>Figure 2.15</b> A resistivity-temperature curve for VO <sub>2</sub> -based ceramics ( $x$ Cu–15VPG–(85- $x$ ) VO <sub>2</sub> ( $x$ =0–15 wt%). The sample had a composition (wt.%), The curves in the figure indicate an amount of Cu added (wt%) : 1) 0; 2) 4; 3) 6; 4) 8; 5) 10; 6) 12 [24]
<b>Figure 3.1</b> The descriptive schematic of a hot press machine where the heat and pressure is applied simultaneously to the sample.
<b>Figure 3.2</b> The descriptive schematic of a density measurement set-up where sample's weight is measured in the air and in the liquid.
<b>Figure 3.3</b> The schematic of spark plasma sintering (SPS) where the punches act as electrodes for current production. [25]
<b>Figure 3.4</b> A set-up diagram for the cryostat sample property measurement where currents are applied to the sample and heater to measure transport properties $\rho$ and $k$ , respectively
<b>Figure 4.1</b> The XRD of commercially available VO <sub>2</sub> compared with the available pure VO <sub>2</sub> 's PDF (#00-043-1051)
Figure 4.2 A phase diagram of VO <sub>x</sub> oxide. [36]
<b>Figure 4.3</b> The XRD scan of a hot-pressed (600°C, 30Mpa for 5 minutes) sample compared to pure VO <sub>2</sub> 's PDF
<b>Figure 4.4</b> The comparison of XRD scans of PECS time-varied samples (sintered for 5, 10, 20, 30, 45 and 60 minutes) to a pure VO <sub>2</sub> PDF
<b>Figure 4.5</b> The comparison of XRD scans of PECS temperature-varied samples (sintered at 600, 700, 800, 900 and 1000°C) to a pure VO <sub>2</sub> PDF. Samples were sintered for 5 minutes
<b>Figure 4.6</b> The resistivity of 30, 45 and 60-minute sintered samples
Figure 4.7 The thermal conductivity, $k$ , of 30, 45 and 60-minute sintered samples
Figure 4.8 The color difference between the samples obtained from (left) SPS (right) Sol-gel . 44
Figure 4.9 The XRD result of the sample obtained from sol-gel technique and the pure VO <sub>2</sub>

<b>Figure 4.10</b> The XRD scans of commercial VO <sub>2</sub> powder ball-milled for a different amount of time (none, 0.5 and 2 hours) before sintering	
<b>Figure 4.11</b> The XRD result for differently ball-milled samples (0.5-hour and 2-hour milled) after sintering	. 47
Figure 4.12 The thermal conductivity, $k$ , data comparison between differently ball-milled samples (none, 0.5 hours, 2 hours)	. 48
<b>Figure 4.13</b> The XRD results of different VO <sub>2</sub> -Cu composites (Cu 2 at%, 3 at%, 4 at%, 5 at% before sintering with a comparison to available PDFs of pure VO <sub>2</sub> and Blossite structure	_
<b>Figure 4.14</b> The XRD results of different VO <sub>2</sub> -Cu composites (Cu 2 at%, 3 at%, 4 at%, 5 at% after sintering with a comparison to available PDFs of pure VO <sub>2</sub> and Blossite structure	-
Figure 4.15 The resistivity, $\rho$ , of various Cu-added samples (Cu 2 at%, 3 at%, 4 at%, 5at%)	. 52
<b>Figure 4.16</b> The pictures of graphite die punches used in SPS for 3 at%, 4 at%, and 5 at% VO <sub>2</sub> Cu composites	_
<b>Figure 4.17</b> The thermal conductivity, $k$ , of the Cu-VO <sub>2</sub> composite samples in the whole temperature region (80K-350K)	. 54
<b>Figure 4.18</b> The thermal conductivity, $\mathbf{k}$ , of various Cu-added samples in the 300K-350K region	. 55

#### **CHAPTER 1. INTRODUCTION**

Currently, electronics are getting smaller and more compact. However, the amount of information processed by the devices has increased tremendously. Moreover, people want their devices to have higher power-efficiency for longer uses.

To achieve a more power-efficient electronic device while maintaining a fast processing speed and compact size, conventional electric circuit components need a breakthrough. One of such components is a transistor.

Transistors control the flow of current inside a circuit to amplify or switch electric signals depending on the application of external voltage.[1] If we can construct a transistor that can switch 'on and off' efficiently at an ultrafast timescale without adding extra components or without complicated algorithms, a breakthrough for a faster yet smaller electronic device would be realized.

In this perspective, insulator metal transition (IMT) phenomena can be found very useful because it typically occurs with a simple electric field or temperature change. Also, this transition occurs through the bulk of crystal thereby freeing the size limit of the device. Thus, there are many works being conducted on realization of IMT-based transistors.[2]

Not only do the electrical properties change through IMT, but also the thermal conductivity should change when a material undergoes a transition from insulator to metal or vice versa. If we can utilize this, an efficient thermal switching device for directing a heat flow or for maintaining a 'set' temperature could be constructed.

It is desirable if we can make this switching occur faster and show a very sharp distinguishable difference between two different states for switching applications.

In this work, the possible applications of vanadium dioxide (VO<sub>2</sub>), a well-known IMT material as a thermal switch was explored. To achieve a much sharper thermal conductivity ( $\mathbf{k}$ ) distinction between the two states for better thermal switching behavior,  $\mathbf{k}$  should be enhanced in the metallic phase while reduced in the insulator phase.

For this purpose, the following was set as the main objectives of this study: (1) synthesizing phase-pure  $VO_2$  with various synthesis methods and conditions; (2) utilizing increased grain boundary scattering to reduce the lattice thermal conductivity on the insulating side of the transition, and (3) utilizing a concept of composite material for better switching behavior of  $VO_2$ .

#### CHAPTER 2. BACKGROUND AND MOTIVATION

#### 2.1 Band theory of solids

When the two atoms are brought closer together, the electron wave functions start overlapping together. The overlapping occurs in constructive or destructive manners. This results in molecular bonding and anti-bonding.[3]

In a crystal lattice, there are countless atom-atom interactions. Therefore, the overlapping of different wave functions will create many different wave curve combinations, leading to accumulation of band splitting. This accumulation of splitting creates a continuous energy bands separated by an 'empty space' in the middle. This empty space is called a forbidden band, an origin of energy band gap. The figure below (**Figure 2.1**) is a descriptive presentation of this phenomenon. Here, hydrogen molecules were used as an example. [4] [5] [6]

The allowed band located below the gap is called a valence band, and the one located above is called a conduction band. Using this energy band theory, conductors, insulators and semiconductors can be differentiated.

In good conductors such as bands are half-filled valence and electrons can move to nearby energy states very easily without requiring much additional energy. [4] On the other hand, a large energy gap exists between the conduction and valence bands in insulators. Thus, electrons cannot move easily without a significantly large potential difference. This makes insulators poor conductors

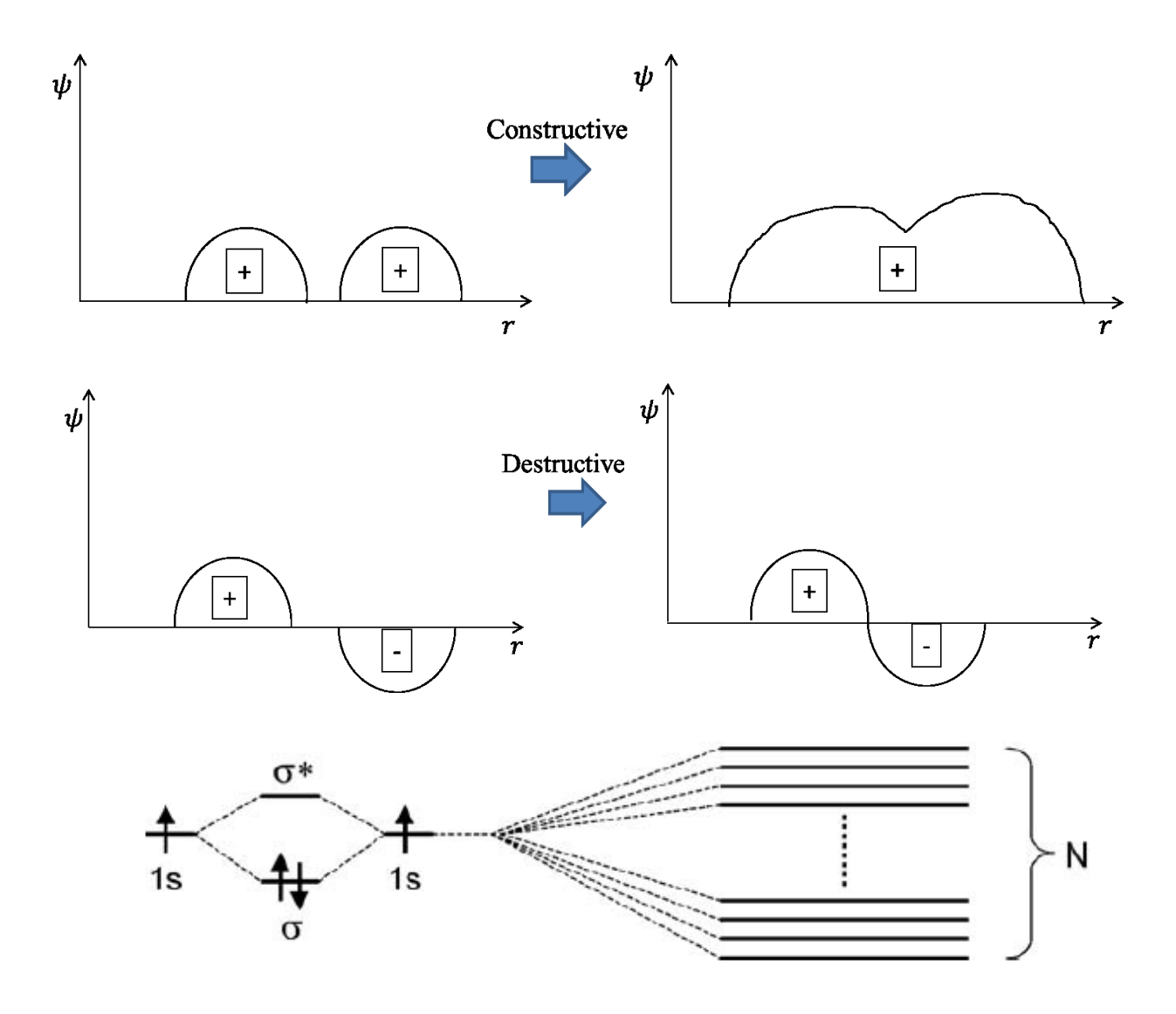


**Figure 2.1** Illustration of atomic energy levels splitting into energy bands when atoms are brought together to form a molecule [5] [6] For interpretation of the references to color in this and all other figures, the reader is referred to the electronic version of this thesis.

## 2.2 Insulator to Metal Transition (IMT) phenomena

According to this classification, there seems to be no connection between an insulator and a metal. However, there are certain materials which show a 'transition' from metal to insulator or vice versa when it reaches a certain temperature or voltage. This is a very interesting phenomenon because such materials can be promising candidates for switching applications.

It is known that IMT can be induced by various triggering mechanisms. Such triggering includes a change in temperatures, pressures, magnetic or electric fields. When IMT occurs, the properties of materials, for example, resistivity or resistance, change accordingly from metals to insulators and vice versa. (**Figure 2.2**) [7] As seen in **Figure 2.2**, the resistance of a sample (in this case, VO<sub>2</sub> thin film) drops by four orders ( $10^5$  to  $10 \Omega$  – cm) undergoing a transition from insulator to metal. This transition is triggered by a temperature change (thermal triggering). The transition temperature of VO<sub>2</sub> is approximately 67°C.

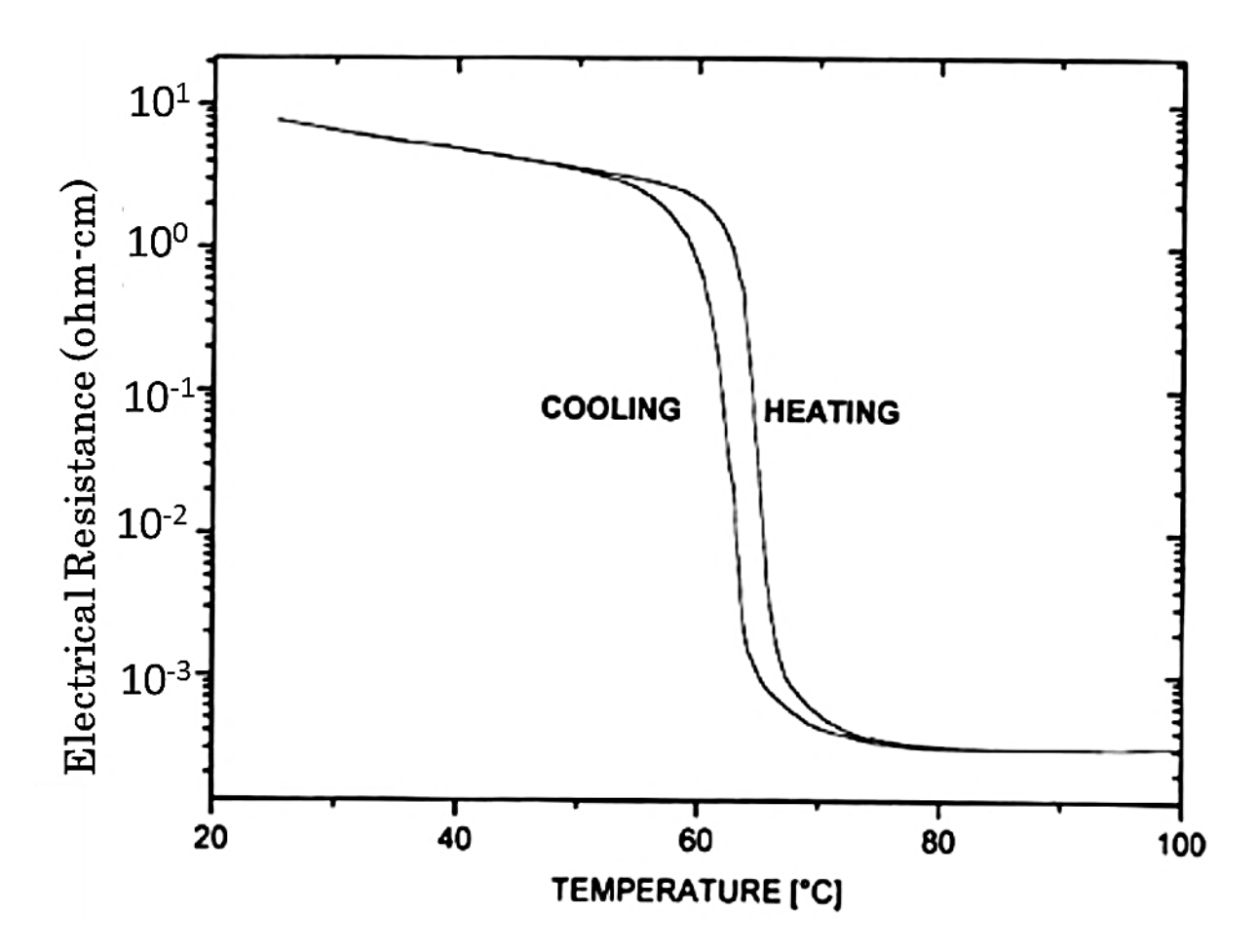


**Figure 2.2** The observation of a sudden drop in resistivity in a 100 nm-thick  $VO_2$  thin-film through IMT. [7]

Optical properties also change through IMT. The following figure (**Figure 2.3**) shows that optical reflectivity increase as a sample is heated through the IMT. Moreover, the optical transmittance percentages change for different wavelengths as  $VO_2$  undergoes a transition.

(Figure 2.4) [7]

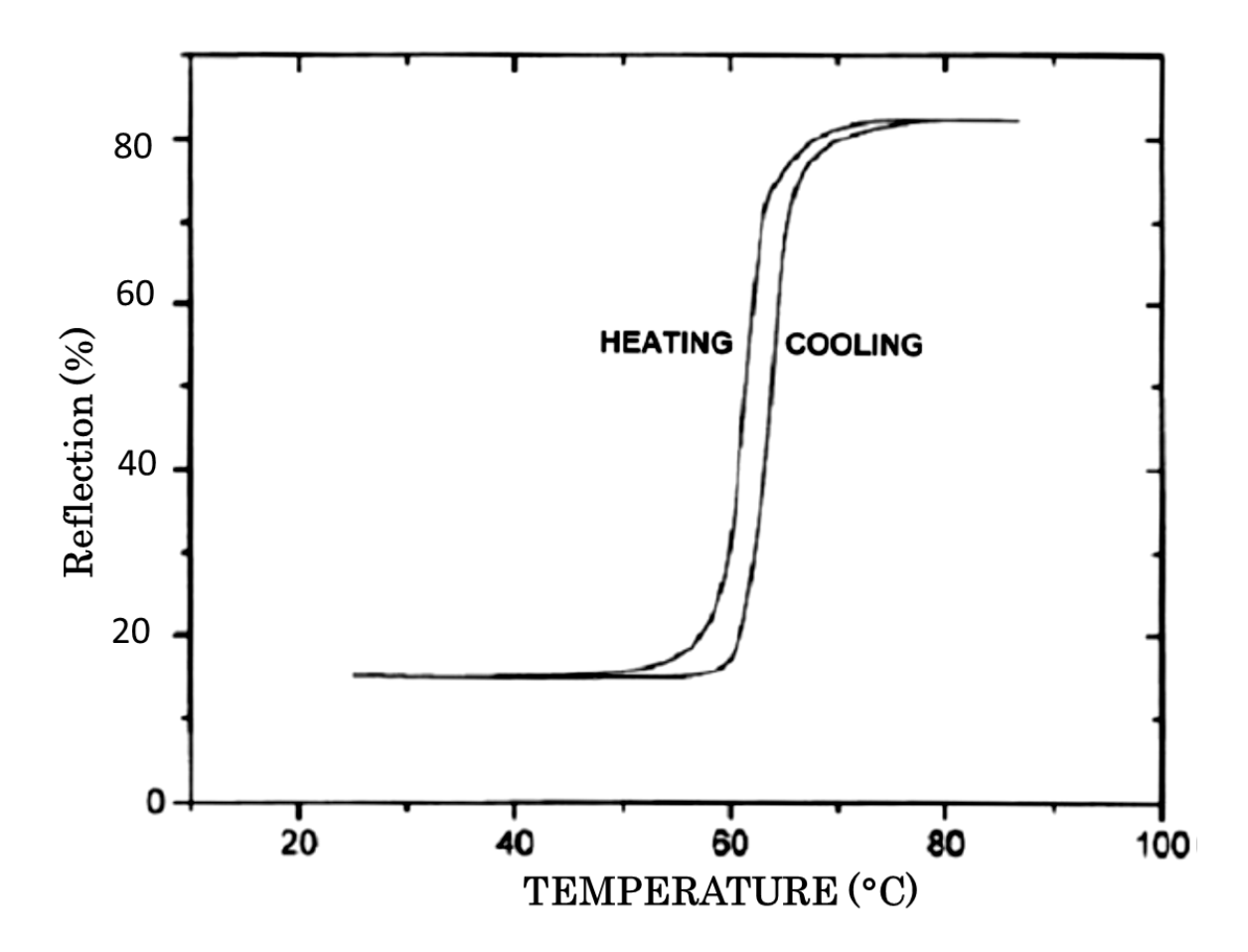


Figure 2.3 The  $VO_2$ 's reflection property change in light reflectivity measured for a 100nm  $VO_2$  thin-film sample. [7]

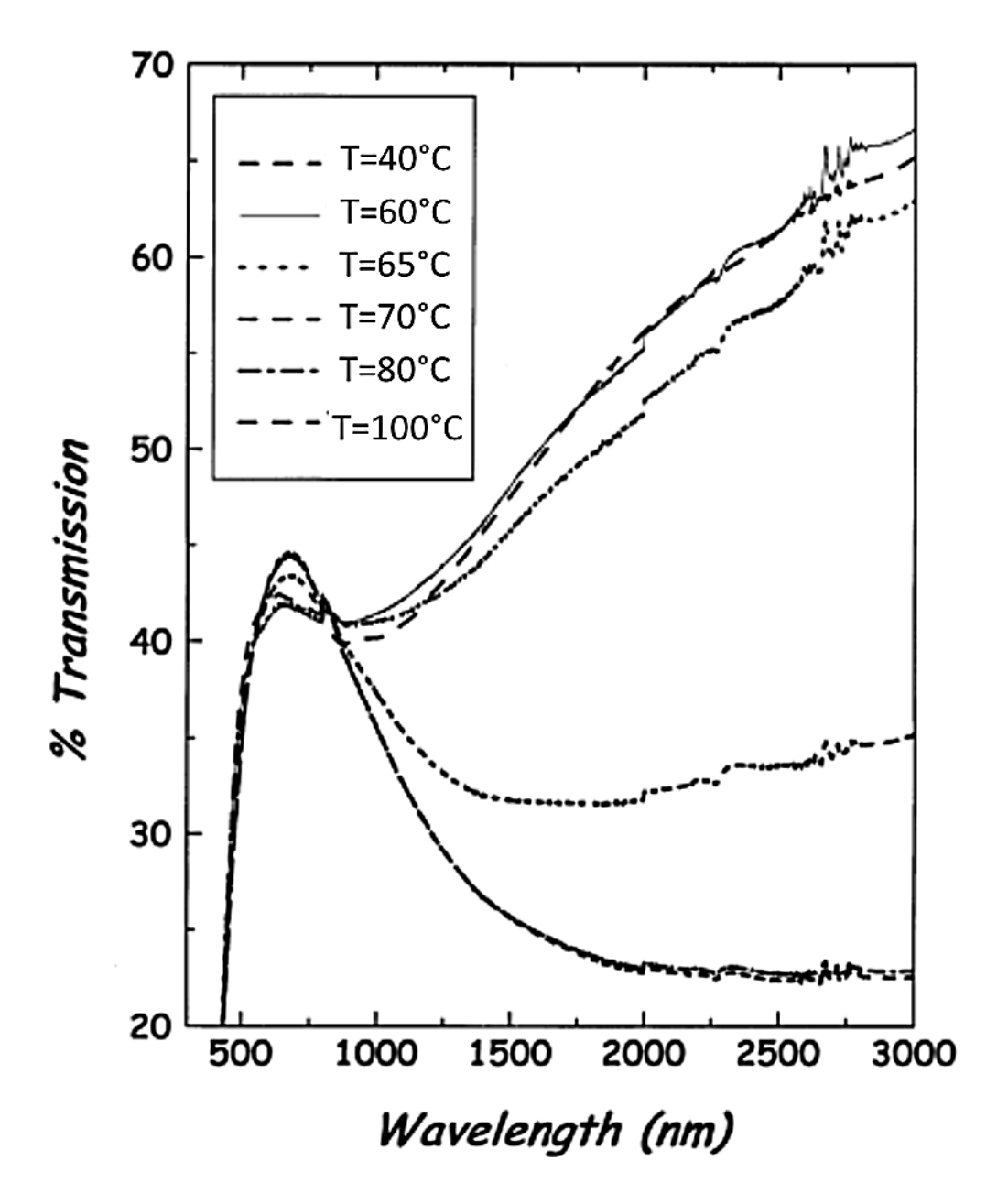


Figure 2.4 The light transmission percentages change for different wavelengths as a  $VO_2$  thinfilm sample deposited onto a sapphire substrate undergoes a transition at 67°C [8]

#### 2.3 Basic IMT mechanisms

Even though IMT phenomenon has been discussed for more than 60 years, the primary mechanism behind IMT is still under debate. Currently, three theories (Mott, Peierls, Anderson) are widely accepted. [9]

According to Mott's theory, when the carrier density exceeds a critical carrier density,  $n_c$  which can be calculated from  $n_c^{1/3}$   $a_H \approx 0.2$  where  $a_H$  is the Bohr radius of the material, the electron-electron interaction such as correlation occurs. He proposed this interaction leads to a phase transition. [10]

If it is assumed conduction happens by hopping of electrons from one site to another in a crystal lattice, the Coulomb repulsion occurs when there is an electron already occupied in the new site. When this repulsion energy U is much greater than electrons' kinetic energy, the electrons would not be able to travel through the lattice. [11]

This localization of electrons leads to a formation of two separate bands, UHB (upper Hubbard band) and LHB (lower Hubbard band), resulting in an insulating phase. This can be converted back to a metallic state by applying stress to shorten the atomic spacing or doping. (**Figure 2.5**)

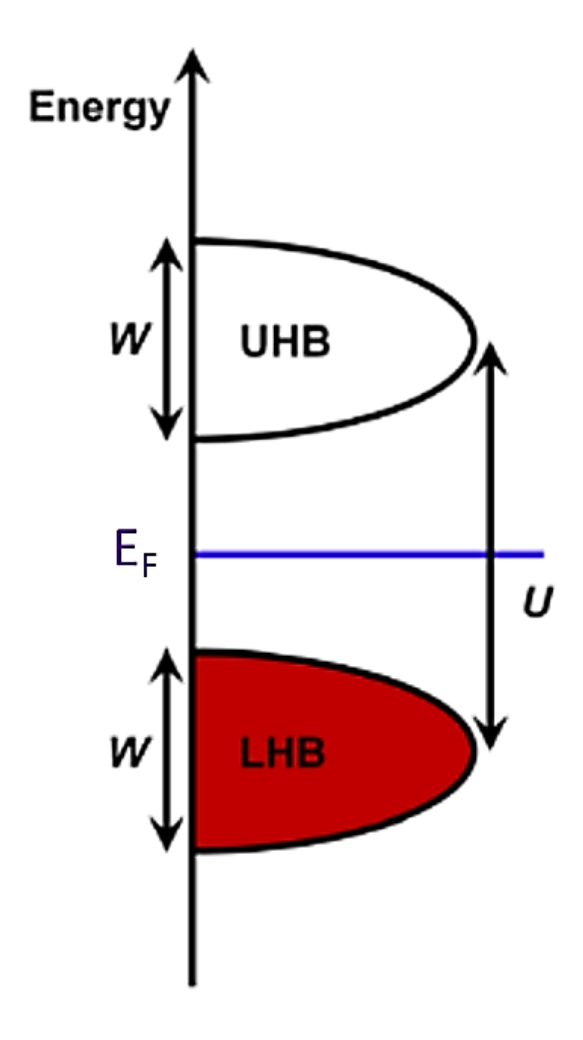


**Figure 2.5** The formation of upper Hubbard band (UHB) and lower Hubbard band (LHB) due to electron correlation [11]

In the second model, Peierls proposed that IMT occurs from a structural change in a lattice of the material. To explain this, a one-dimensional metal with a lattice constant,  $\boldsymbol{a}$ , and an even atomic displacement of  $\boldsymbol{L_0}$  can be assumed. When a distortion of the periodic chain happens as shown in **Figure 2.6**, it causes a change in a repeat distance to  $\boldsymbol{L'}$ . Then, the new zone boundary forms at  $\boldsymbol{\pi/L'}$  where a band opening occurs as depicted in **Figure 2.6**.

Because of this gap creation, the energy of electrons near the Fermi surface is reduced.

This reduction in energy counteracts with the energy gain from elastic energy required for lattice deformation. Thus, when one exceeds another, the transition occurs. [11]

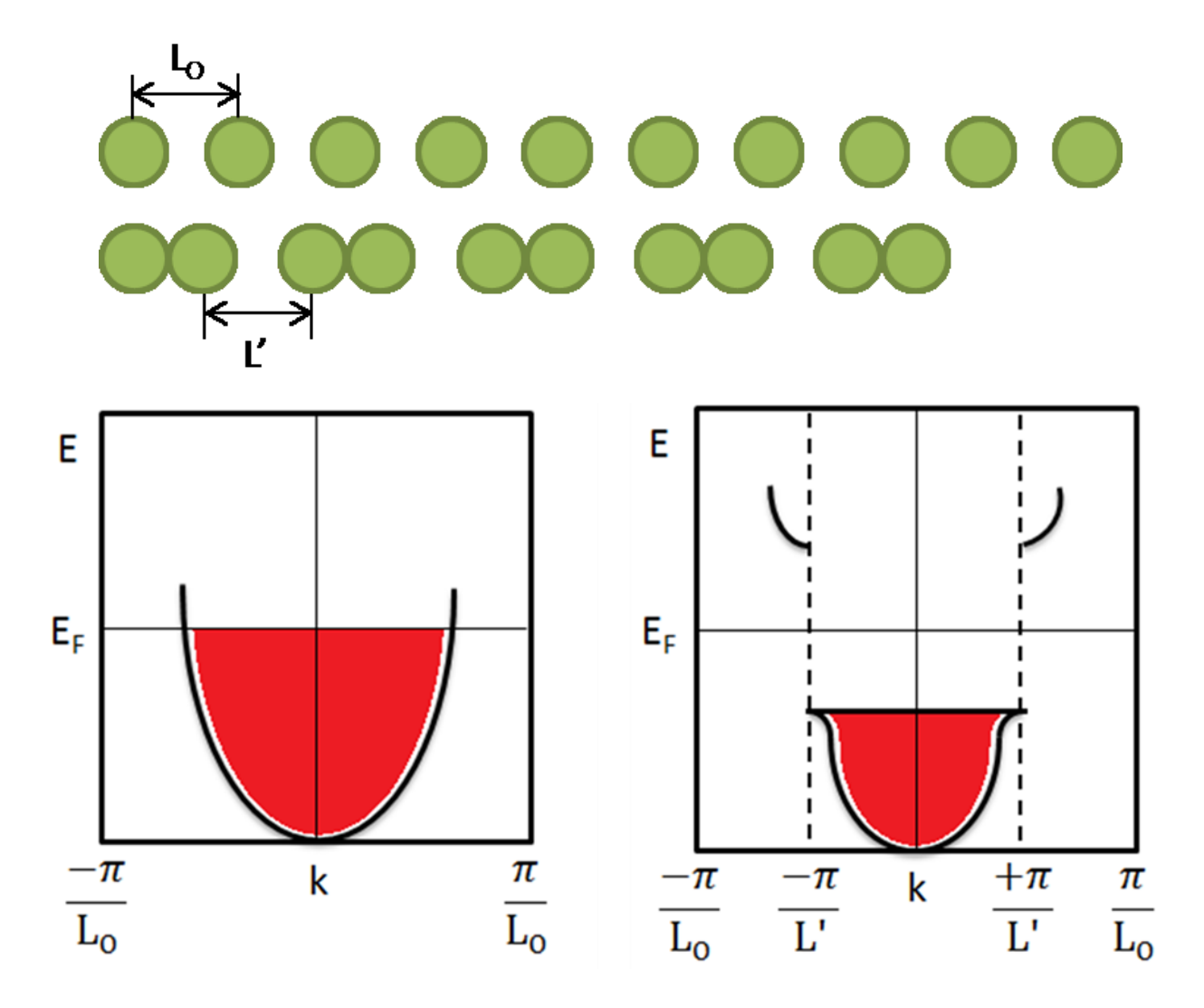


**Figure 2.6** The 1-D atomic configuration of normal lattice and the distorted lattice, and the corresponding electronic band structures of normal and distorted lattice respectively. [11]

In the third model, Anderson tried to explain IMT using disorder-induced localization effect. He proposed that randomly distributed defects in a lattice such as impurities or vacancies can impact conductivity by scattering conducting electrons in the lattice. These defects or disorders in a system create uneven lattice potentials causing separation of localized and

extended states as seen in **Figure 2.7**. [11]  $E_c$ , the mobility edge, defines the boundary between localized and extends states. The movement of Fermi energy, either below or above  $E_c$ , causes a transition.[12]

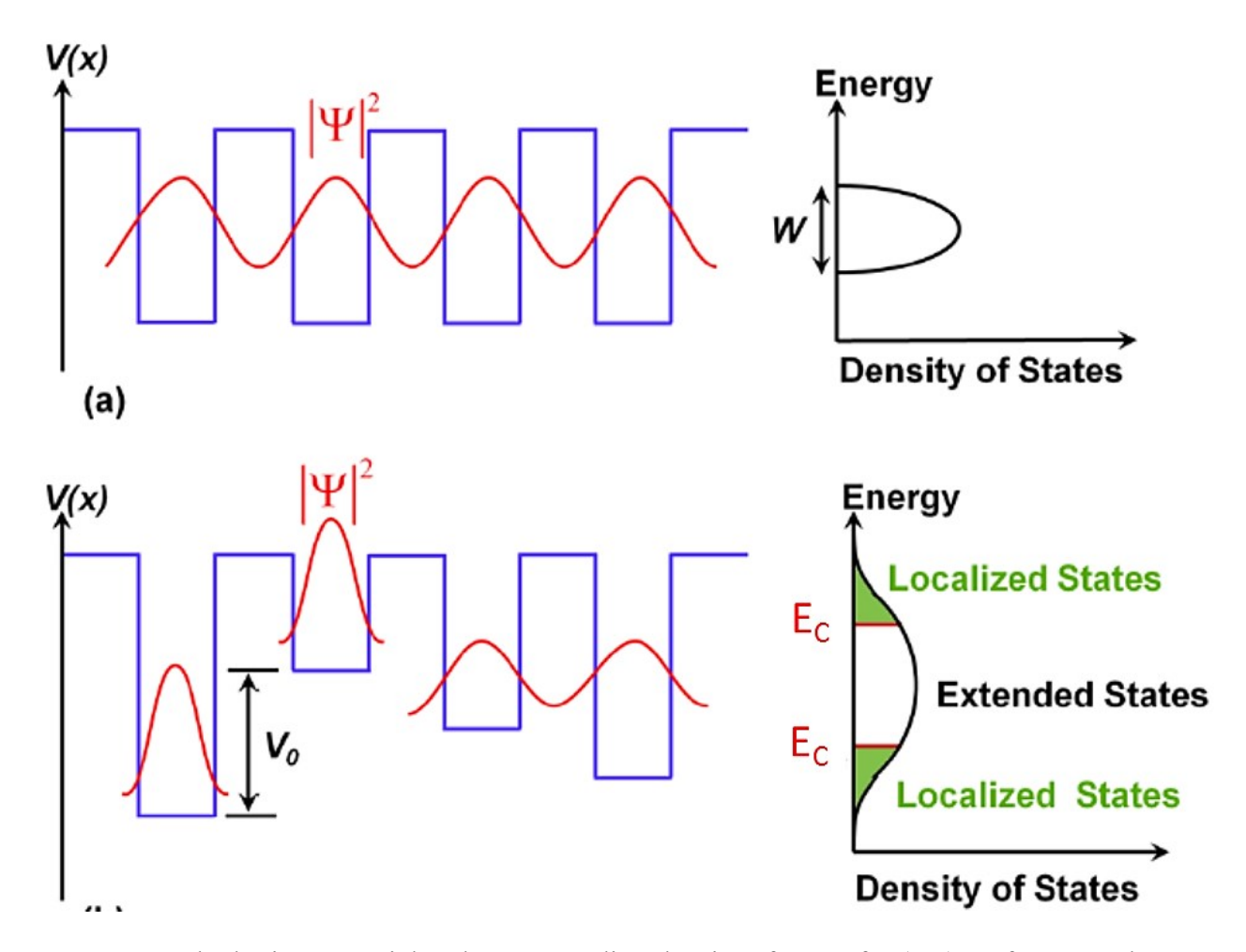


**Figure 2.7** The lattice potential and corresponding density of states for (top) perfect crystal And (bottom) disordered crystal. [11]

Unfortunately, scientists are currently divided on determining whether IMT in  $VO_2$  is induced by structure change (Peierls type) or the carrier reactions (Mott-Hubbard type).

## 2.4 Applications of IMT

The applications of IMT materials are quite diverse. This is due to IMT materials' abilities to exhibit an extraordinarily large property changes at an ultrafast time scale. By utilizing these abilities we can develop a very efficient and cost-effective switching material system.

For example, in an electric-electronic system, a high-speed noise signal having a higher voltage than the appropriate level can destroy the system by entering the system from the power source. In this case, IMT materials exhibiting transitions to insulators above a certain high voltage level can save the system by bypassing those higher-voltage noise signals in the circuit at ultrafast timescales. [13]

It was actually observed in thin-film VO<sub>2</sub> samples, the resistance of the sample suddenly increases at a certain critical voltage. (**Figure 2.8**) [14] By manipulating this critical voltage level through doping or modification of thin-film dimensions, one can selectively choose a voltage level where high-voltage noise signals will bypass the circuit. This type of applications can be used in household electronics, electrical substations, for instance.

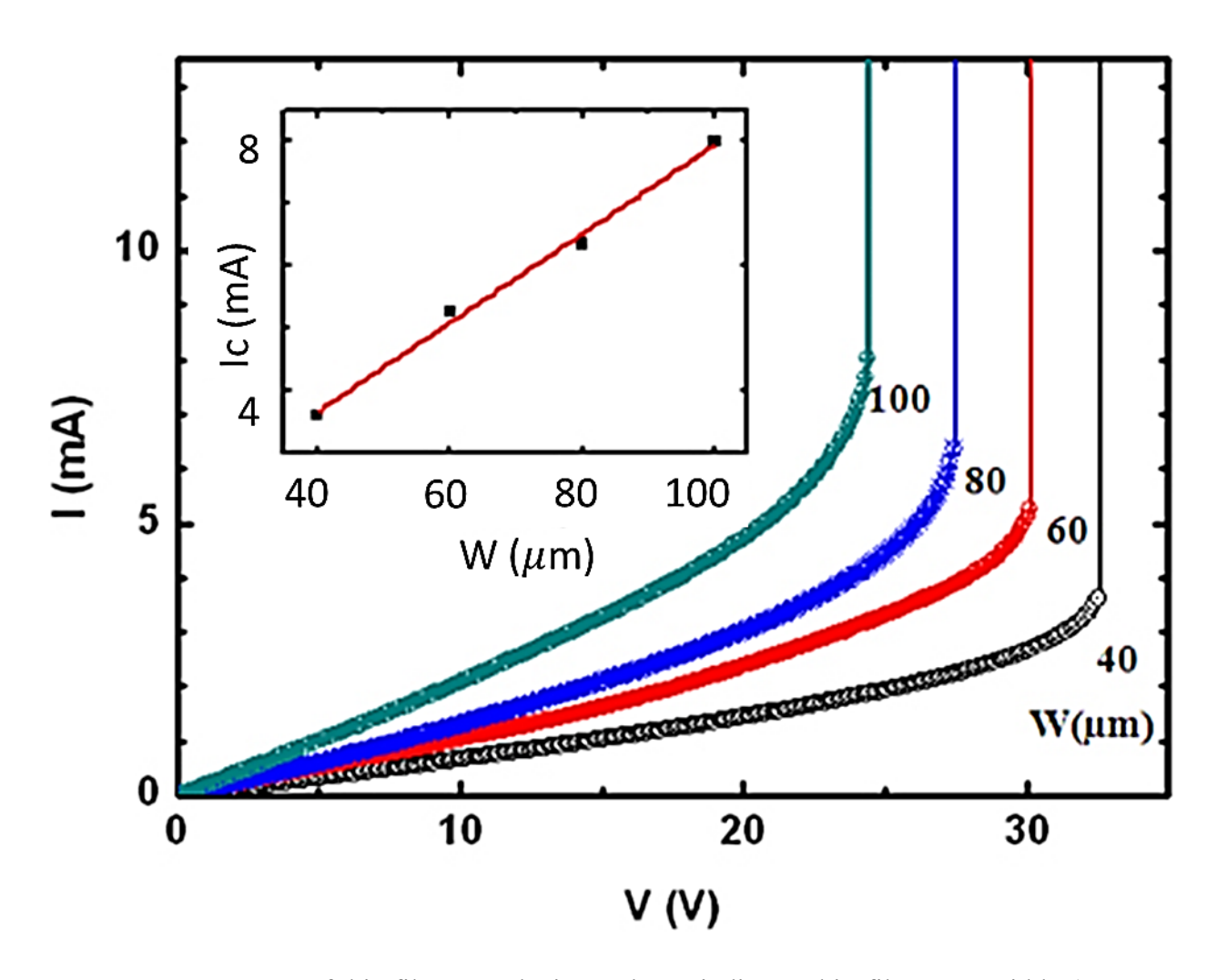


**Figure 2.8** I-V curves of thin film  $VO_2$  devices. The W indicates thin-film mesa width. (40, 60, 80 and 100  $\mu$ m were used) The inset shows the critical current fitted for different W values. [14]

Additional promising application can be found in Li-ion batteries. Recently, the explosive nature of Li-ion batteries, especially those used for cell-phones, has drawn much interest from the public. In batteries, there is a device called Positive Temperature Coefficient of Resistance (PTCR) that protects a circuit from short-circuit or overcurrent by blocking the current flow when the battery is overheated. The electron charges in the blocked current become more unstable at higher temperatures thereby increasing the internal pressure inside the battery cell. This will eventually cause the battery to explode.[15]

In this case, an IMT material can be a good solution. Once the cell phone is overheated, an IMT-material based explosion prevention device will turn into a metal from an insulator. This conductive metallic phase will allow the built-up charges inside the battery to be discharged before explosion. This idea can be applied to laptop batteries as well. [16]

This concept was actually tested by a research group at ETRI (Electronics and Telecommunications Research Institute) in South Korea. **Figure 2.9** below shows that when an IMT-based device was used in a cell-phone battery (the right-hand side picture), it does not explode even at 210°C because it allows a dissipation of accumulated current in the battery. Also, the swelling of a battery was reduced from 42% to 22% with the IMT-based device. Their experimental result published for Korean media was translated into English. [33]

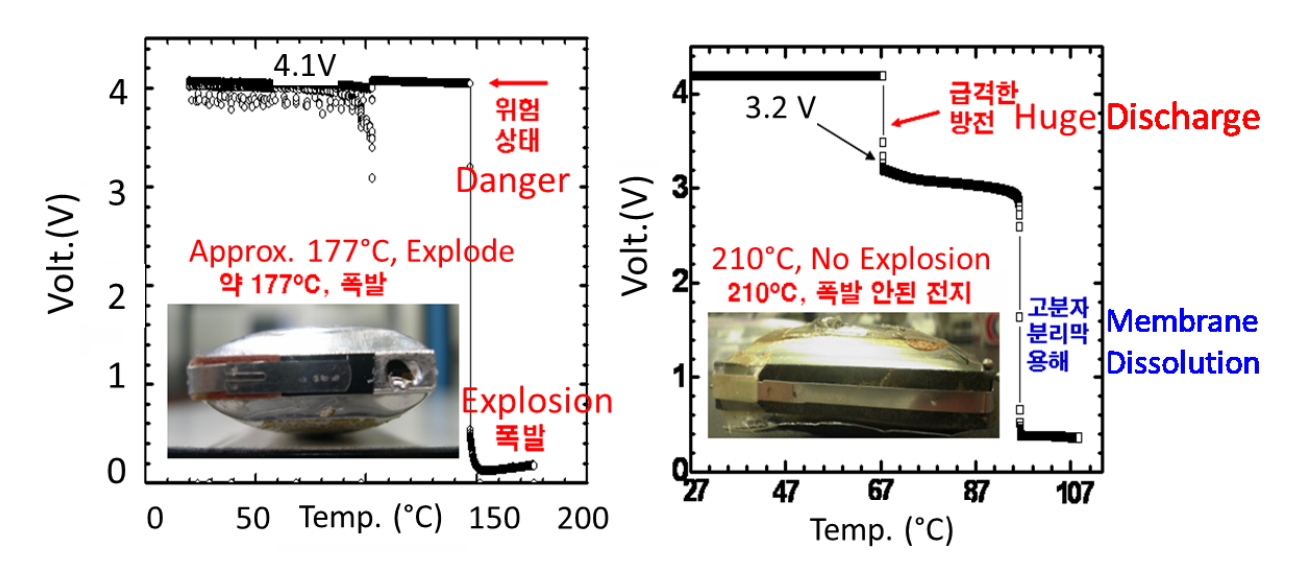


**Figure 2.9** A cell phone (a) without and (b) with a VO<sub>2</sub>-based device in a cell phone to prevent battery explosion. [33]

Applications in thermochromic windows have been extensively researched as well. It is known that optical transmittance properties changes through thermal-triggering of IMT. In case of VO<sub>2</sub>, the amount of light reflection increases as it undergoes a transition from insulator to

metal as seen in Figure 2.3-(a). [7, 8]

Therefore, when the temperature is low as it would be in the winter time, the IMT coating on glass will allow more light to pass through to maintain warmness in the building. The situation will be reversed in the summer time when the IMT coating on glass will reflect most of the light to cool the inside of the building.

It is also important to note that when VO<sub>2</sub> changes to a metallic state at a high temperature, most of the infrared-region (IR) light (longer wavelengths) is reflected as shown in **Figure 2.3-(b)**. [8] On the other hand, shorter wavelength-light transmittance at a metallic state remains almost the same through the transition. This special property enables the thermochromic windows let a sufficient light pass through while selectively blocking infrared radiation-induced heat at higher temperatures.

## 2.5 Thermal switching

Thermal switching applications, our work interest, have been investigated hardly at all in comparison to electronic switching or thermochromic applications. However, a system dynamically changing its thermal conductivity to the surrounding atmosphere will be an interesting research subject for its applications in self-regulated heat flow device.

Moreover, since IMT can passively control the heat flow without using thermostats or specific programs, the power and costs required to operate conventional heat flow directors can be saved. Thus, this type of thermal switch can be found very useful in an area where power source is limited. A spacecraft operating with a limited amount of resources in space can be one example.

As shown in Figure 2.10 below, a thermal (heat) switch based on IMT material is

installed between electronics and spacecraft structure such as panel or radiator, which will act as a cold sink. When the temperature of the electronics increases above the set-point temperature, it needs to dissipate the heat for safety. Here, the IMT material will transit into a metallic state, increasing the thermal conductivity and thus allowing the excess heat to dissipate to the radiator and out to space through the switch easily. As the temperature cools down below the set-point temperature, the IMT material will transit back into an insulator state having a lower thermal conductivity. This will prevent the temperature of electronic components from getting affected by the temperature variation in spacecraft structure. Therefore, one can maintain an operation-conductive temperature of electronics regardless of ambient heat variations without extra power requirements. [17]



**Figure 2.10** A thermal switch controlling the temperature of electronics device in a spacecraft [17]

It is obvious the efficiency of this thermal switch will be significantly improved if such device can switch between two states extremely rapidly with a much sharper distinction between the two states. In this work, the latter goal, a sharper distinction, is sought.

While the electrical properties of IMT materials have been studied in great detail, the behavior of the thermal conductivity across such triggering is less well understood.

It is known that the thermal conductivity (k) is composed of two terms; electronic and lattice thermal conductivity. The electronic thermal conductivity term ( $k_{elec}$ ) evolves from the

electrons carrying not only the charge, but also thermal energy. The lattice thermal conductivity term  $(k_{lat})$  describes heat carried by phonons, quanta of lattice vibrations. The following equations are generally used to calculate each component.

$$k = k_{elec.} + k_{lat.} \quad (2.1)$$

$$k_{elec.} = \sigma L T$$
 (2.2)

$$k_{lat.} = \frac{1}{3}Cvl \tag{2.3}$$

where  $\sigma$  is electrical conductivity,  $\boldsymbol{L}$  is the Lorenz number, T is the temperature,  $\boldsymbol{C}$  is the specific heat per unit volume,  $\boldsymbol{v}$  is the sound velocity and  $\boldsymbol{l}$  is the phonon mean free path. [18] Equation (2.2) relating the electrical and thermal conductivities is known as the Wiedmann-Franz relation.

Since electrons are not free in insulators, the lattice component will be more dominant for thermal conductivity than the electrical one in insulators. The case is reversed in metals because there are many free electrons available for conduction.

The key to developing IMT-based thermal switching is to design the material such that two conditions are achieved: 1)  $k_{lat}$ . is small throughout the entire temperature range, but especially below the transition; and 2)  $k_{elec}$ . dominates in the metallic state. If these conditions are met, then as the material passes from the low temperature insulating state to the high temperature metallic state, the thermal conductivity will transition from small (lattice dominated) to large (electron dominated).

## 2.6 Vanadium dioxide for thermal switching

Among various IMT oxides,  $VO_2$  has been a main focus of many scientists because when it undergoes an IMT, a drastic drop in electrical resistivity or resistance (an order of  $10^4$  or  $10^5$ ) occurs at a picosecond time scale as seen in **Figure 2.2**. The IMT happens approximately at 67 °C for  $VO_2$ .

This electrical property change is accompanied and driven by with a change in crystal structure. It has been known that the crystal structure of  $VO_2$  changes from monoclinic (insulator state below  $T_{MIT}$ ) to tetragonal rutile (metal state above  $T_{MIT}$ ) during IMT. [10, 19, 20]

Consequently the electronic band structure of  $VO_2$  changes as well to reflect a transition from metal to insulator state. (**Figure 2.11**)

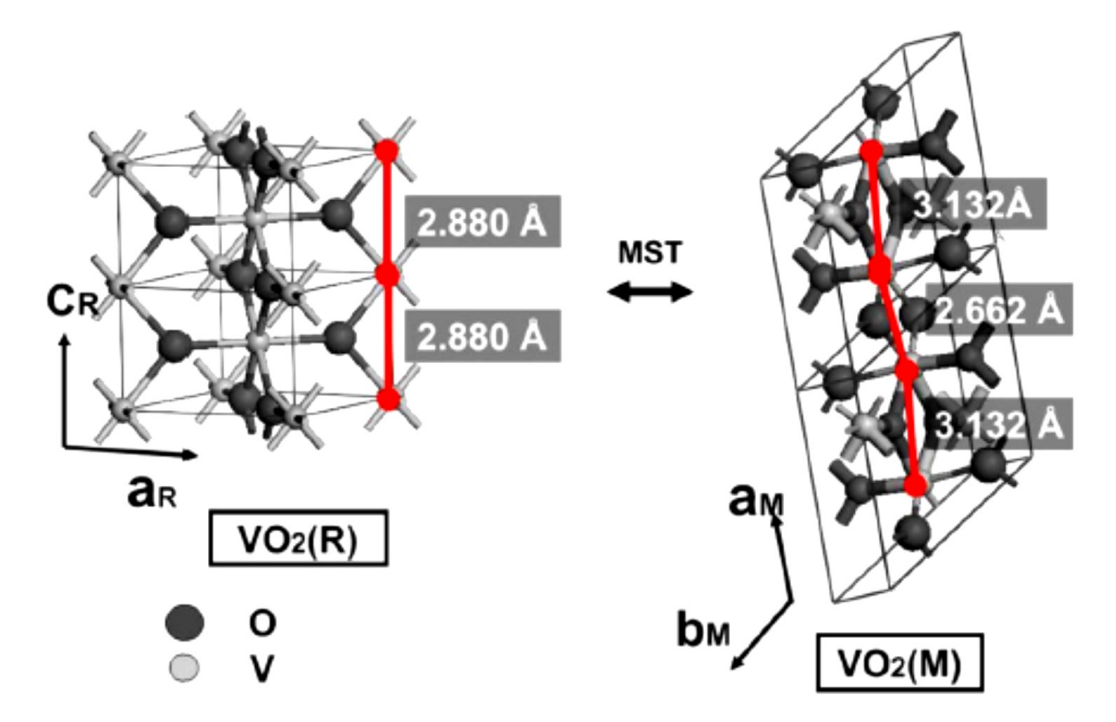


Figure 2.11 The unit-cell structure of  $VO_2$  (left) after and (right) before transition. "MST" stands for metal to semiconductor transition. [20]

There have been only a few reports of the behaviors of the thermal conductivity of VO<sub>2</sub> across the IMT. **Figure 2.12-(a)** shows a plot of thermal conductivity vs. temperature for a thin-film VO<sub>2</sub> sample. [21] **Figure 2.12-(b)** shows the thermal conductivity change through IMT in a bulk-form VO<sub>2</sub> sample analyzed by Berglund in 1969. [22] Here, we can see that the degree of thermal conductivity change is much lower in a bulk sample than in a thin-film sample. Moreover, compared to the five orders of magnitude change in resistivity, the magnitude of change in thermal conductivity needs to be improved for better switching behavior.

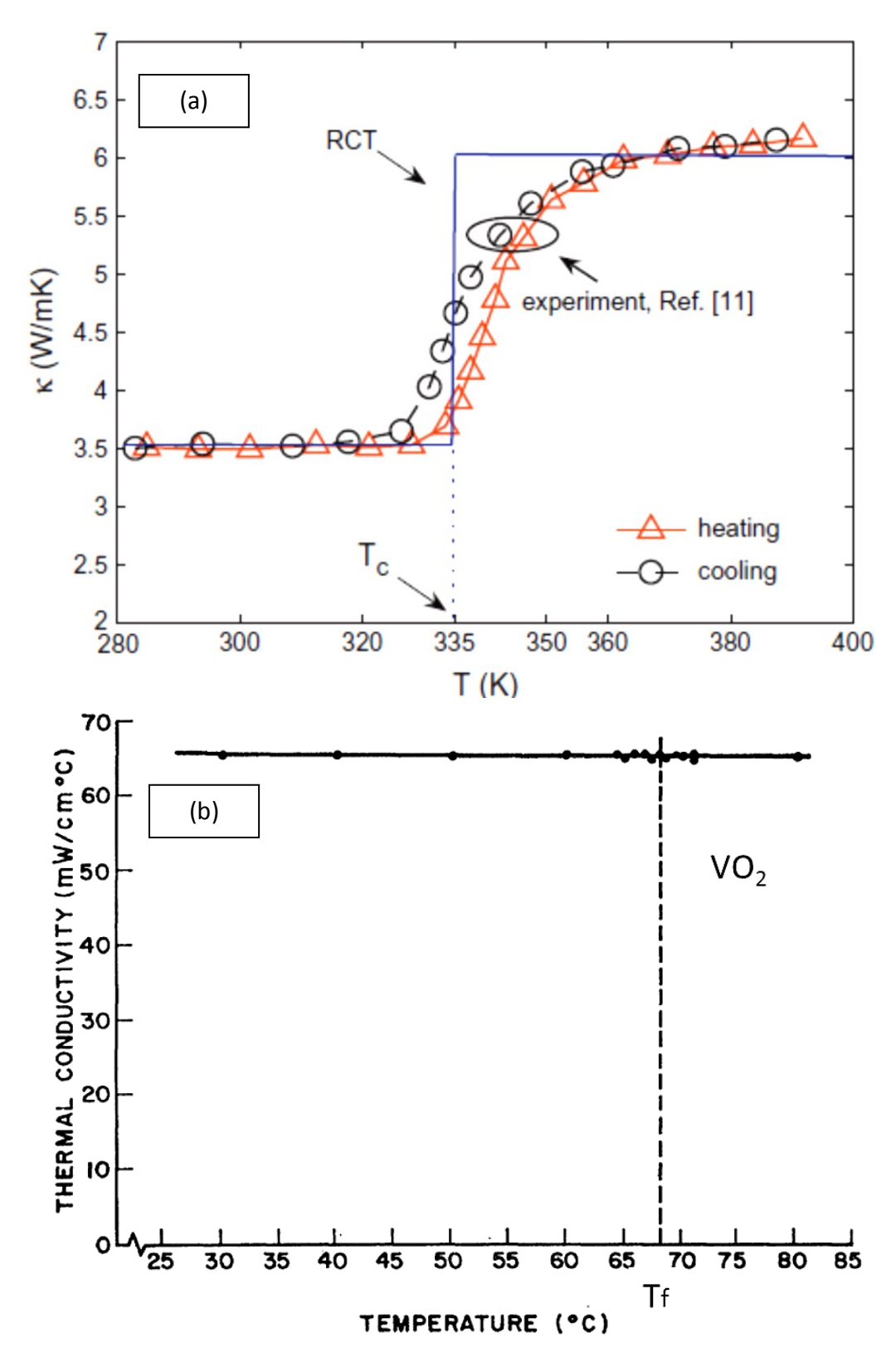
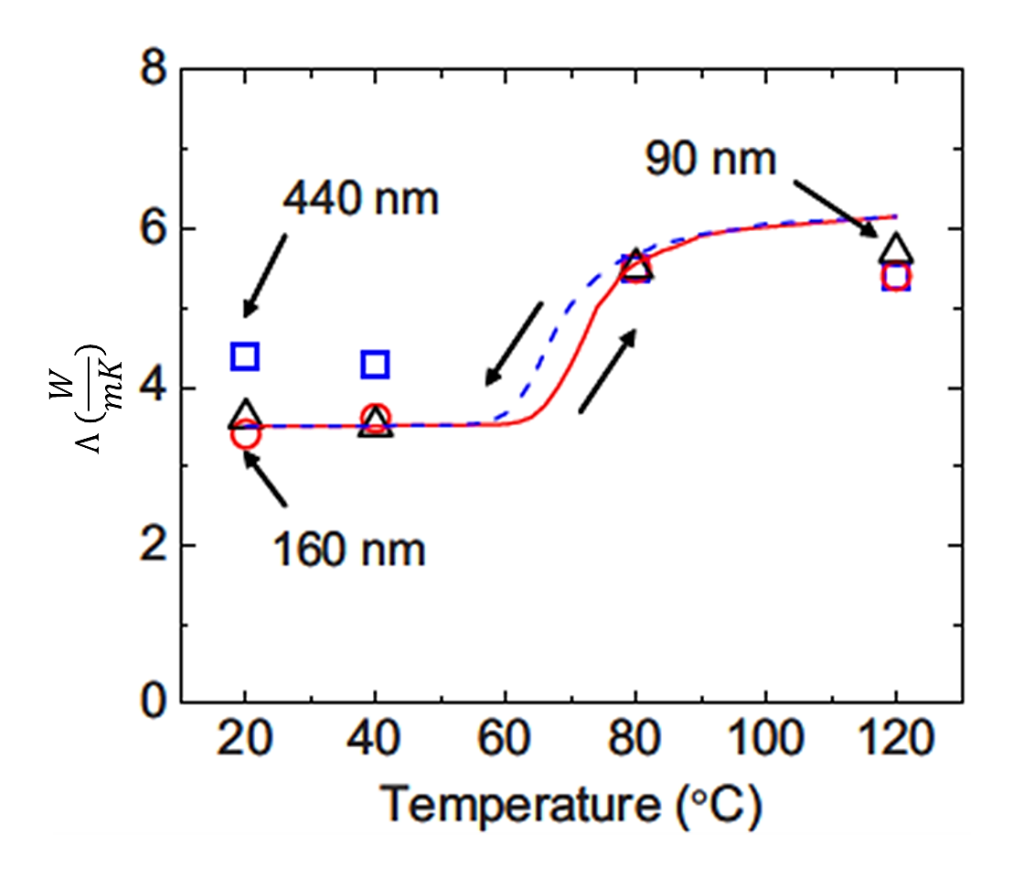


Figure 2.12 A VO<sub>2</sub> thermal conductivity, k, curve in (a) thin-film (b) bulk form. In (a), the red triangle-line indicates the values obtained when heating and the black one from cooling. [21,22]

As specified in Section 2.5, for better switching behavior,  $k_{lat}$  in the insulating phase should be reduced while  $k_{elec}$  at a metal phase should be increased.

One of the common methods to decrease  $k_{lat}$  is decreasing the grain-size of a system. It was actually shown that the k of VO<sub>2</sub> thin-film decreases at a lower temperature region when the film thickness which is directly proportional to grain size decreases from 440 nm to 160 nm (**Figure 2.13**). [23] These results suggest that synthesizing specimens with nano-sized grains may be an effective approach to reducing  $k_{lat}$ .



**Figure 2.13** A VO<sub>2</sub> thin-film thermal conductivity curve. The numbers indicate the film thickness. [23]

However, enhancing transition in thermal conductivity is still challenging, and it is known that a general class of materials exhibits a change in k by a factor of ten with a change in temperature. [35]

Enhancement in *k<sub>elec</sub>*. in the metallic region is more difficult. However, one possible approach is to adopt a composite concept. Here, good electron-conducting metals such as copper are added to a VO<sub>2</sub> matrix to form a composite material. When VO<sub>2</sub> matrix is an insulating phase at a lower temperature, the copper particles are separated by insulating VO<sub>2</sub> matrix thereby preventing electron flow and electronic thermal conductivity. However, when the matrix transitions to a metal phase at a higher temperature, the whole system is now metallic and thus the highly conductive copper inclusion will contribute to an increase in thermal conductivity. A brief schematic showing this concept is presented below. (Figure 2.14)

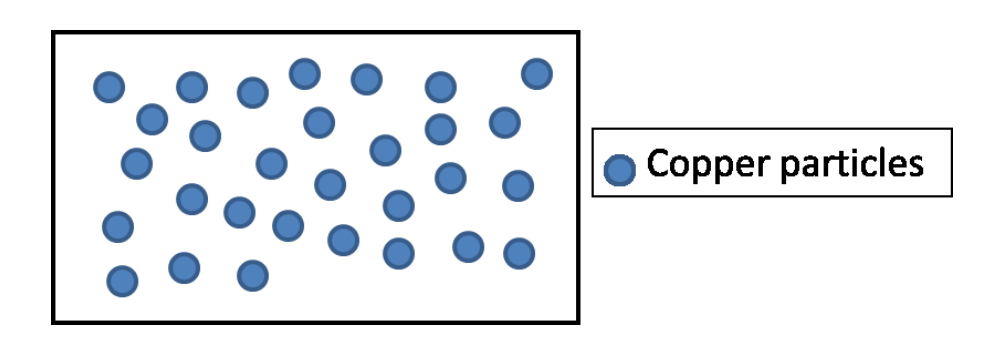


**Figure 2.14** A descriptive schematic of an intended VO<sub>2</sub>-copper composite. The blue dots indicate copper particle inclusions inside the VO<sub>2</sub> matrix

This concept of adding highly conductive metal particles to  $VO_2$  matrix was actually tried by Kolbunov et.al in 2003. [24] In their experiment, they used vanadium dioxide-based ceramics having a composition of xCu–(85-x)  $VO_2$  –15VPG (where VPG—vanadium phosphate

glass of composition (mol%)  $80V_2O_5-20P_2O_5$ ) to investigate how electrical resistivity changes as the amount of copper additives,  $\boldsymbol{x}$ , change. The following figure (**Figure 2.15**) shows their experimental result.

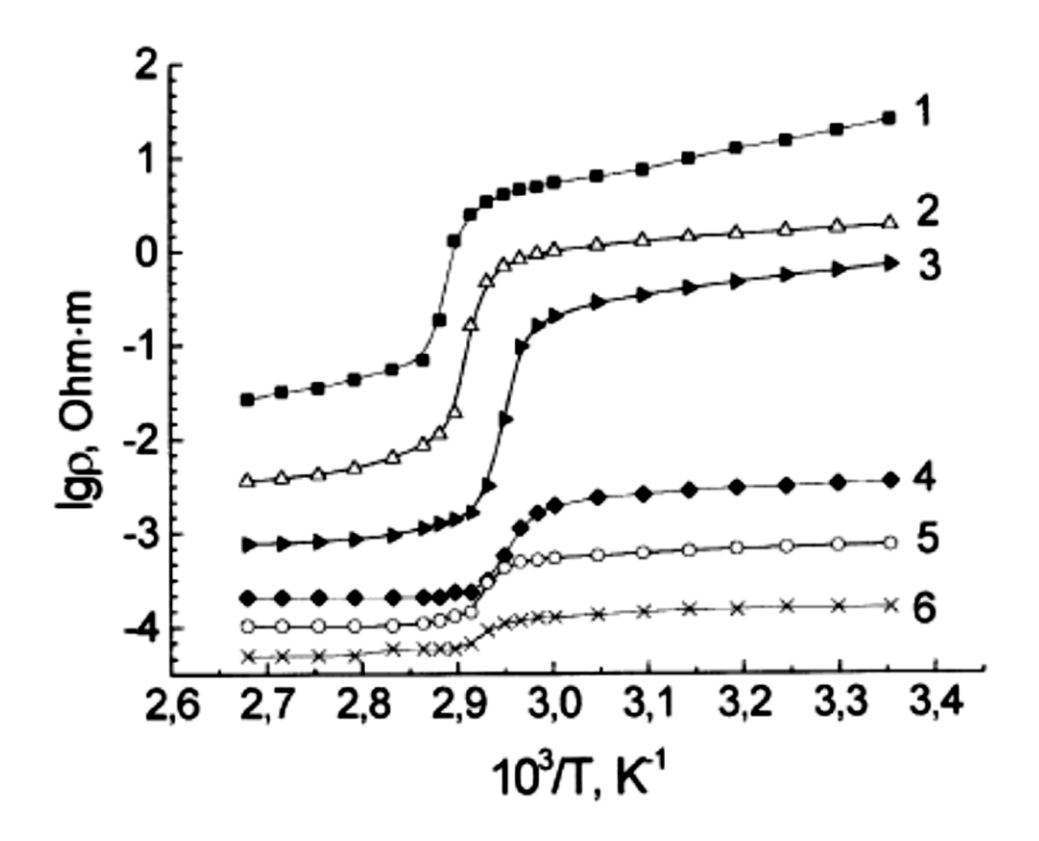


**Figure 2.15** A resistivity-temperature curve for VO<sub>2</sub>-based ceramics (xCu–15VPG–(85-x) VO<sub>2</sub> (x=0–15 wt%). The sample had a composition (wt.%), The curves in the figure indicate an amount of Cu added (wt%) : 1) 0; 2) 4; 3) 6; 4) 8; 5) 10; 6) 12 [24]

It was found that for the highest copper concentration (12wt %) (curve #6), the resitivity exhibited a sizeable decrease in resistivity compared to pure VO<sub>2</sub> (curve #1). This large increase in  $\sigma$ , electrical conductivity, is desirable because according to the Wiedemann-Franz law (equation (2)), a higher electrical conductivity yields a higher value of electronic thermal

conductivity. Thus, an increase in  $\sigma$  due to these conductive metal particles would yield an increase in  $k_{elec}$  at high temperatures.

In designing such composites is, however, care must be taken to ensure that copper particles are not going to agglomerate in the matrix because this agglomeration could produce high conductivity even in the low temperature region where we require the material to be insulating.

#### 2.7 Summary

The switching behavior of IMT materials is potentially very interesting and useful for modern electronics. Due to their ability to change their electrical properties in the bulk form significantly at a very small timescale, electronic components, especially transistors, can be substantially improved in their signal switching ability and power requirement.

More detailed study of the thermal properties, such as thermal conductivity, of IMT materials may allow the development of a very efficient thermal switching device. Applications of thermal switches will enable effective control of the temperature automatically without requiring any additional power resources. This can be useful in spacecraft operations or power plant operations in which power efficiency is very critical.

For this purpose, VO<sub>2</sub> was chosen as a target material in this study because of its rapid reaction to ambient triggering with an extremely drastic property change. Even though this drastic change has not been observed in thermal conductivity, k, measurement, if we were to reduce  $k_{lat}$ . through reduction in grain size and enhance  $k_{elec}$  by adopting a carefully designed highly conductive composite concept, the thermal switching efficiency could be substantially improved.

#### **CHAPTER 3. METHODS AND PROCEDURES**

Based on information and motivation provided in pervious chapters, we tried to synthesize a bulk  $VO_2$  sample to see whether it can be used as a potential thermal switch. For this, we first synthesized pure bulk  $VO_2$  as a reference, and then conducted ball-milling for reduction of  $k_{lat}$ , and synthesized Cu-VO<sub>2</sub> composites for enhancement of  $k_{elec}$ .

## 3.1 Synthesizing pure VO<sub>2</sub>

To synthesize bulk-form pure  $VO_2$  samples, hot-pressing, spark plasma sintering (SPS) and a sol-gel technique were attempted.

#### i) Materials

## (1) Hot Pressing and Spark Plasma Sintering

The 99%-pure metal basis VO<sub>2</sub> powder (Product #22957, Alfa Aesar, Ward Hill, MA, United States) was used for synthesizing a bulk-form VO<sub>2</sub>. The particle size was -100mesh and it was stored inside the vacuum glove box to prevent oxidation.

#### (2) Sol-Gel Technique

For sol-gel technique, 1.2 ml of Vanadium Triisopropoxide oxide (VO[OCH(CH<sub>3</sub>)<sub>2</sub>]<sub>3</sub>), a precursor material, (Product #470783, Alfa Aesar, Ward Hill, MA, United States) and a solvent, composed of 8.6 ml of acetone and 3.6ml of water were prepared.

#### i) Procedures

#### (1) Hot Pressing

The first sintering method used was hot pressing. Here, 2.5 grams of the commercial VO<sub>2</sub> powder was pressed into a pellet form under the application of heat and pressure in an inert argon atmosphere. The sintering temperature was set at 600°C while the pressure level was maintained at 30MPa. The powder was placed into the graphite die and held under this condition for approximately 5 minutes. Insulating foam was placed between a heater and the graphite die to minimize the heat loss.

Subsequently, the system was allowed to cool to ambient. After the sample reached a room temperature, the 'puck' was taken out for further analysis. The descriptive schematic of a hot press system is presented below. (**Figure 3.1**)

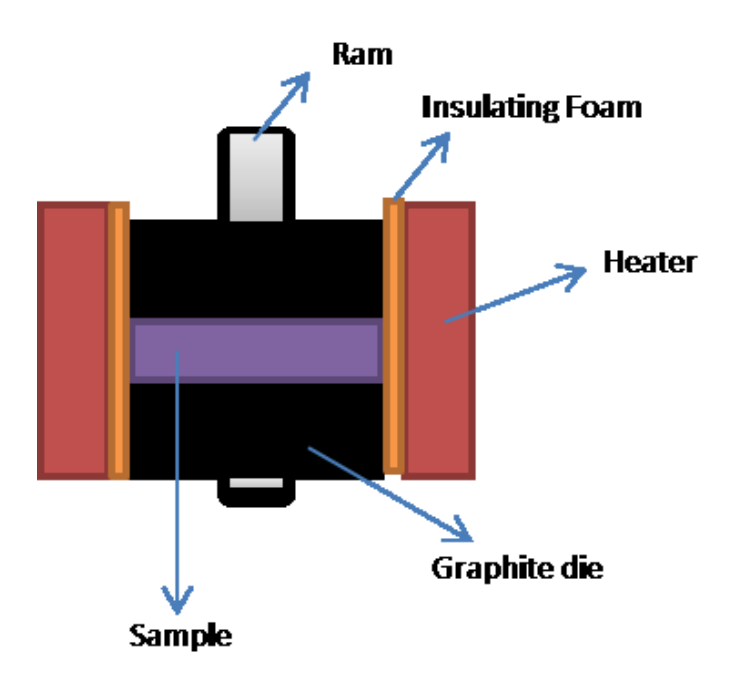


**Figure 3.1** The descriptive schematic of a hot press machine where the heat and pressure is applied simultaneously to the sample.

The density of a sample was measured based on Archimedes' Principle. It states that the weight of the liquid displaced by an immersed object is equal to the upward force, called 'buoyancy', exerting on the object. Based on this, the density of a solid can be measured using a balance specially set up as shown in **Figure 3.2**. [34]

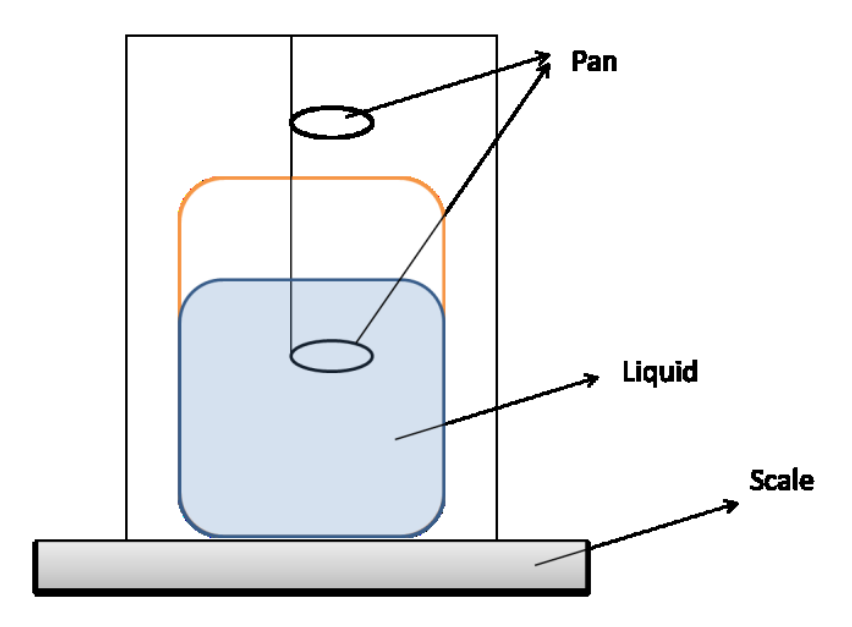


**Figure 3.2** The descriptive schematic of a density measurement set-up where sample's weight is measured in the air and in the liquid.

First, the sample's weight in the air was measured by placing it on the top pan. Then, after zeroing out the scale, the sample was placed in the bottom pan immersed in the liquid. The weight value would be negative. Finally, the following equation was used to measure the density.

$$\rho = \frac{A}{|B|} \times \rho_0$$

where  $\rho$  is the density of sample, A is the sample's weight in the air, B is the weight in liquid and  $\rho_0$  is the density of liquid. In this experiment, ethanol was used as an immersing liquid. [34]

Following the density measurement, the samples were subjected to XRD to confirm phase purity. For this, a sample was first ground to a fine powder from using a mortar and a

pestle. It was then spread on a glass-slide and placed inside an XRD machine (Rigaku MiniFlex II model). When operating, the machine will collect the intensities of diffracted x-ray beam at different rotating angles. The resultant scan result was compared to previously established result, referred to as the PDF-database. If the sample was indeed a single-phase  $VO_2$ , transport properties (resistivity,  $\rho$  and thermal conductivity, k) were conducted.

## (2) Spark Plasma Sintering

The second method for pellet synthesis was spark plasma sintering (SPS). One type of SPS systems available at Michigan State University is the Pulsed Electric Current Sintering (PECS) system (Model SPS 10-3, Thermal Technology LLC, Santa Rosa, CA, United States).

The critical sintering parameters were temperature and sintering time, and studies were carried out to observe whether longer sintering time and higher sintering temperature were beneficial in terms of phase purity and sample density.

In SPS, the powder form of the sample is placed in a graphite die and the pulsed DC current flows through the particles, producing Joule heating. The current flow is produced by using one punch as an anode and another as a cathode. Due to heat produced from this current flow, the diffusion of the atoms between the particles will be promoted resulting in consolidation. The sintering was performed in an inert atmosphere provided by argon gas. The pressure is applied to the sample while heating using the punches.

The die used for compaction in this experiment had a 12.7-mm diameter. The amount of powder used was 2.5 grams. The following diagram shows a descriptive schematic of SPS machine. [25] (**Figure 3.3**)

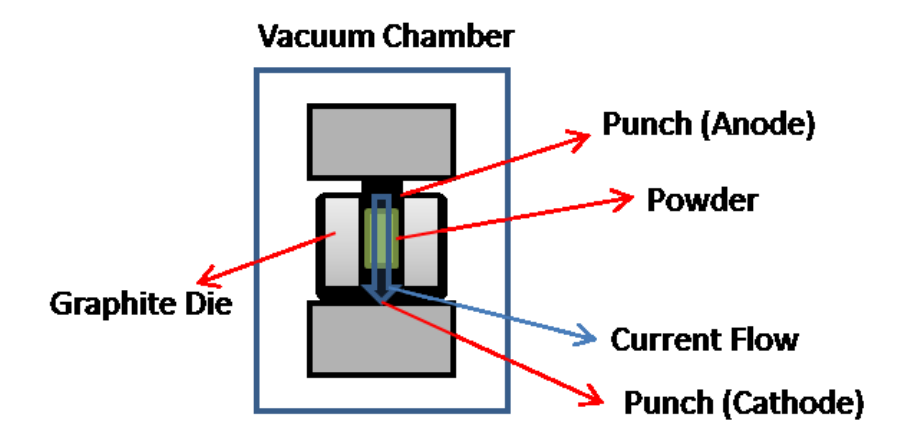


**Figure 3.3** The schematic of spark plasma sintering (SPS) where the punches act as electrodes for current production. [25]

The table below (**Table 3.1**) summarizes the sintering conditions used in this experiment.

**Table 3.1** The temperature and time variations in SPS for pure VO<sub>2</sub> synthesis

Parameter Change	Temperature (°C)	Pressure (MPa)	Sintering Time (Min)
Temperature	600	60	5
	700	60	5
	800	60	5
	900	60	5
	1000	60	5
Time	900	60	5
	900	60	10
	900	60	20
	900	60	30
	900	60	45
	900	60	60

Following the density measurement, the samples were subjected to XRD to confirm phase purity. Only those samples turned out to be a single-phase VO<sub>2</sub> from XRD were then subjected to transport property measurement (resistivity,  $\rho$  and thermal conductivity, k).

## (3) Sol-Gel Technique

The vanadium-containing precursor was mixed with a mixture of water / acetone. This mixture was then chilled with ice for 15 minutes. The gelation occurred rapidly during this procedure. The obtained gel (xerogel) was composed of  $V_2O_5$ . It was then aged for two days in the air to enhance densification.

Typically, to release any trapped solvents such as water or acetone out of pores of the  $V_2O_5$  gel while retaining its structure, supercritical drying is used to get the trapped solvents out safely. The final structure without any solvents remaining is called an 'aerogel'.

However, in this experiment, the first gel sample was dried in the air for a practice run. After two days, the gel dried in a solid form. This sample was then pulverized to a fine powder using a mortar and a pestle to be placed in a furnace at a reducing atmosphere (forming gas of 93% Ar and 7% H). The sample was held at 500°C for approximately 10 hours in the furnace, allowing it to be reduced to VO<sub>2</sub>.

Following the density measurement, the sample was subjected to XRD to confirm phase purity. If it turned out to be a single-phase VO<sub>2</sub>, transport properties (resistivity,  $\rho$  and thermal conductivity, k) were conducted.

### (4) High-Energy Ball Milling

To reduce  $k_{lat}$ . in the insulating region for a better thermal switching behavior, a high-energy ball milling machine (SPEX Mixer/Mill 8000M model, United States) was used. The XRD scans of each differently milled sample were analyzed before they were subject to SPS. For SPS, the sintering temperature was set at 900°C, the pressure at 60MPa and the time for 30 minutes.

A table below (**Table 3.2**) shows a set of different ball milling parameters, mainly ball milling time, used in this experiment. The milling media were stainless steel balls and the milling jar was also made out of stainless steel.

**Table 3.2** The time-variations in ball-milling and sintering parameters for each sample

Ball milling time (Hrs.)	Sintering Temperature (°C)	Sintering Pressure (MPa)	Sintering Time (Min)
None	900	60	30
0.5	900	60	30
2	900	60	30

After measuring the density, the SPS-obtained pellet samples were analyzed by XRD scans for phase purity. It was followed by cryostat measurement for transport properties (only thermal conductivity, k).

# 3.2 Synthesizing VO<sub>2</sub>-Cu Composites

#### i) Materials

For Cu-composites, the 99.9%-pure 20-50nm sized Cu nano-powder (Product # 45504, Alfa Aesar, Ward Hill, MA, United States) was used for the inclusion material. It was stored inside a glove box to prevent oxidation.

### ii) Procedures

First, different amounts (2, 3, 4 and 5 atomic %) of Cu were added to the VO<sub>2</sub> powder.

This mixture was then ball-milled for 30 minutes to promote homogeneity before being subjected to SPS. The following table (**Table 3.3**) summarizes the amounts of Cu and VO<sub>2</sub> that were used for this synthesis.

**Table 3.3** The compositions and amounts used to synthesize VO<sub>2</sub>-Cu composites

Sample Compositions (at%)	VO <sub>2</sub> amount (g)	Cu amount (g)
98 VO <sub>2</sub> – 2 Cu	2.000	0.034
97 VO <sub>2</sub> – 3 Cu	2.000	0.053
96 VO <sub>2</sub> – 4 Cu	2.000	0.071
95VO <sub>2</sub> – 5 Cu	2.000	0.089

One thing to note is that the amount of Cu addition actually used was 10 percent higher than the intended atomic percentage value because upon milling some of the Cu powders tended to stick to the wall of a stainless-steel ball-milling jar.

For SPS, the sintering temperature was set at 900°C, the pressure at 60MPa and the time for 30 minutes. The pellet samples' densities were measured and the XRD scans before and after SPS were collected for each pellet. Finally, the transport properties were measured using the cryostat.

# 3.3 Transport Property Measurements

After obtaining the pellet-form samples from various sintering methods, they were cut in few sections using the diamond saw cutting machine. The cut sample was then set up the following way before mounting. (**Figure 3.4**) Once mounted, the data were analyzed using the appropriate equations.

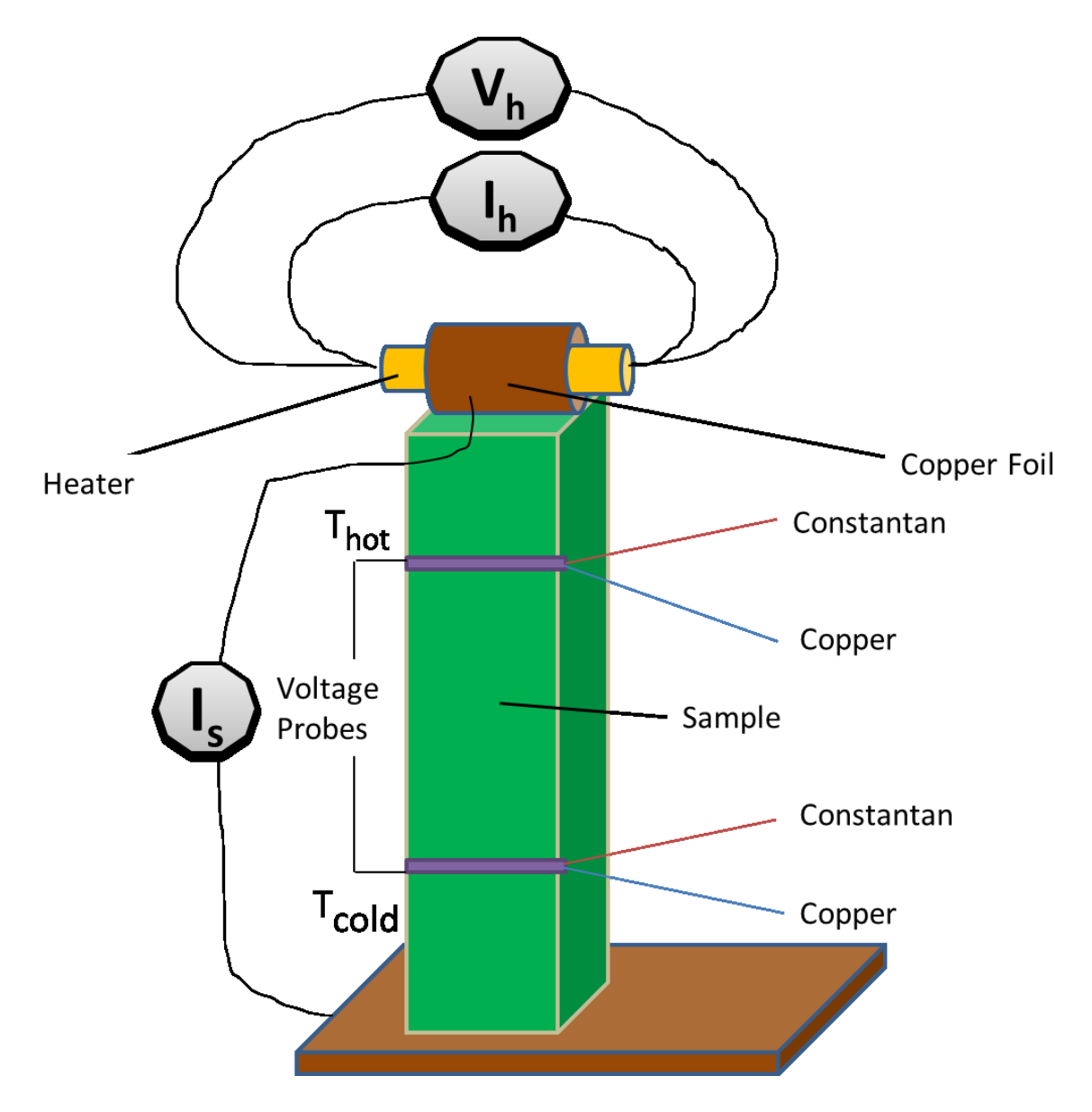


**Figure 3.4** A set-up diagram for the cryostat sample property measurement where currents are applied to the sample and heater to measure transport properties  $\rho$  and k, respectively.

After the sample base temperature is stabilized, current  $I_s$  is passed through the sample, and the voltage across the two copper leads of the thermocouple is measured. The electrical conductivity is determined using Equation 3.1 below.

$$\sigma = \frac{1}{\rho} = \frac{I_S}{\Delta V} \cdot \frac{L}{A} \tag{3.1}$$

The sample current is then turned off, and current  $I_h$  is energized through the sample heater, an  $800\Omega$  resistor on the top of the sample. With this current supply, the heating element will produce heat based on Joule heating. Due to this heat production, a temperature gradient will develop throughout the sample (hot and cold sides).

Temperature  $T_{hot}$  and  $T_{cold}(\Delta T = T_{hot} - T_{cold})$  are determined by measuring the voltage across the two thermocouples fixed along the sample. Thermal conductivity,  $\kappa$ , is then determined using the following relation. (Equation 3.2)

$$\kappa = \frac{PL}{A\Delta T} = \frac{I_h L V_h}{A\Delta T}$$
 (3.2)

where A, the sample cross-sectional area, P, the power, L, the length between the probes,  $I_h$ , the heater current,  $V_h$ , the heater voltage and  $\Delta T$  is the temperature difference between the two probes. When analyzing the  $\kappa$  data, thermal loss caused by radiation was taken into account.

## **CHAPTER 4. RESULTS AND DISCUSSION**

# 4.1 VO<sub>2</sub> Synthesis

# i) Hot Pressed Specimens

The commercial  $VO_2$  was subjected to XRD before any synthesis as an initial purity check. The XRD result (**Figure 4.1**) showed that it is not in a pure single phase  $VO_2$  form. The impurity-phase peaks were identified with  $\blacktriangledown$  marks. The specific phases these impurity peaks belong to could not be identified.

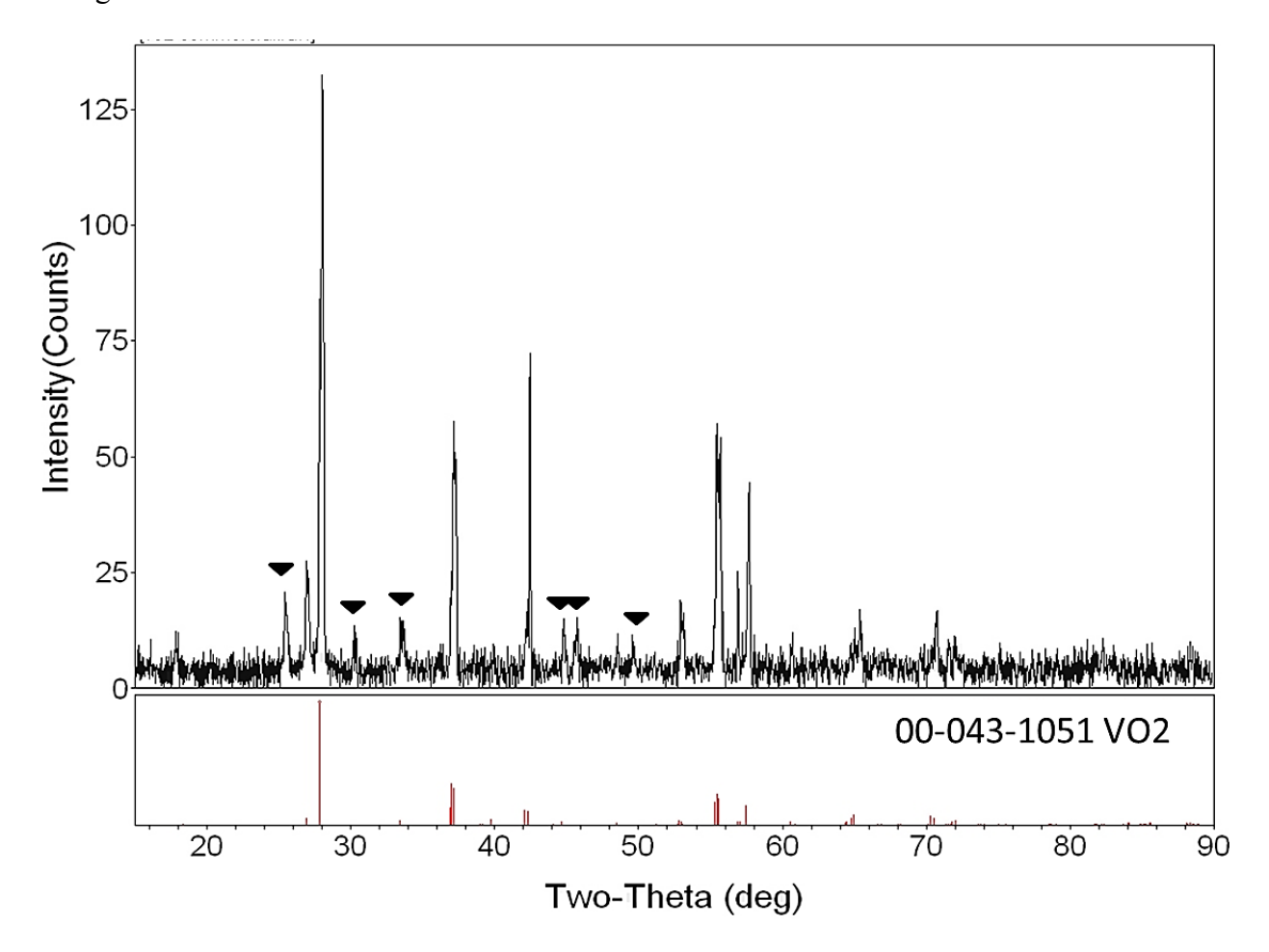


**Figure 4.1** The XRD of commercially available  $VO_2$  compared with the available pure  $VO_2$ 's PDF (#00-043-1051).

This could be attributed to VO<sub>2</sub>'s sensitivity to non-stoichiometry. The phase diagram of VO<sub>x</sub>-oxide (**Figure 4.2**) shows that obtaining a pure single-phase VO<sub>2</sub> can be very challenging due to its high susceptibility to oxygen. Thus, even slight oxidization or reduction during synthesis can inhibit one from obtaining a single-phase VO<sub>2</sub>. [10]

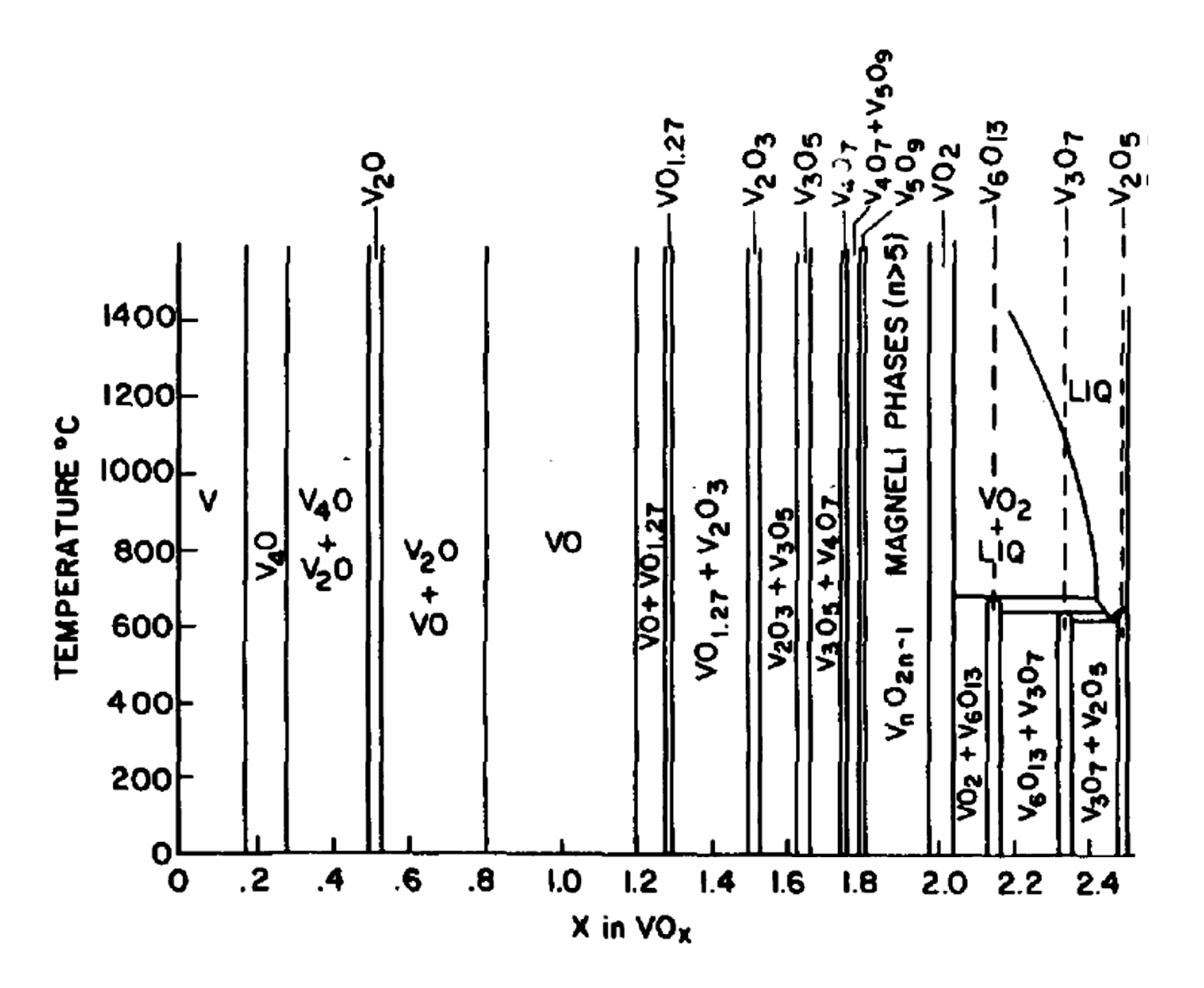


**Figure 4.2** A phase diagram of VO<sub>x</sub> oxide. [36]

Though the powder was not in a single phase form, we attempted hot pressing to study whether it might convert to  $VO_2$  after subjecting the sample to temperature and pressure.

From hot-pressing, the pellet-form sample was obtained and the density was measured. The density was found to be  $3.97 \mathrm{g/cm}^3$ . Since the theoretical density of  $VO_2$  is  $4.57 \mathrm{g/cm}^3$ , the relative density is about 87% of the theoretical value. This is not entirely a poor value, but it was lower than the expectation. The possible reason for the low relative density could be attributed a very high melting temperature of  $VO_2$ , 1,967°C. This is significantly higher than our hot press temperature of  $VO_2$ .

An XRD scan was conducted to see if a hot press method yielded a single phase sample. The result is presented below. (**Figure 4.3**) From this, it was found that hot pressing method did not yield a reasonable single-phase VO<sub>2</sub>. The phases of impurity peaks marked with ▼ could not be identified. Again, it could be attributed to a low operating temperature of the hot press. Since the temperature of our hot press cannot exceed 600°C due to technical issues, this synthesis method was not pursued further after the first experiment.

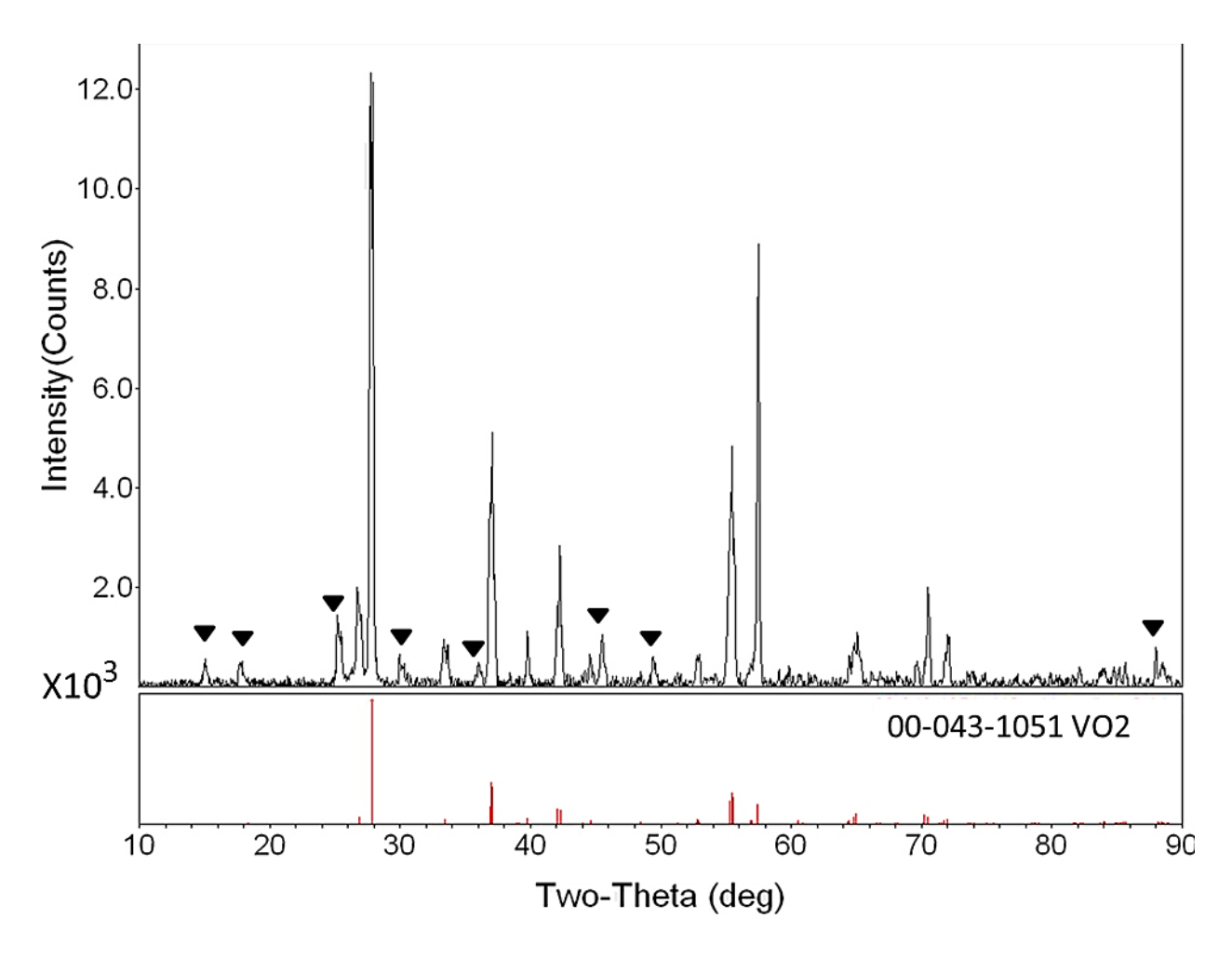


**Figure 4.3** The XRD scan of a hot-pressed (600°C, 30Mpa for 5 minutes) sample compared to pure VO<sub>2</sub>'s PDF

### ii) Spark Plasma Sintered Specimens

The SPS differs from conventional hot press in a way that the heat is generated internally from pulsed DC current passing through the graphite die as opposed to hot press where heat is supplied from an external source. Because of this internal heating, an allowable temperature is much higher than that for hot pressing. In addition, the heat ramping and cooling rates are very rapid. Also, one can vary the die pressure for compaction as well as the sintering time.

The following table (**Table 4.1**) shows the various sintering conditions used in this experiment and relative densities for each sample obtained under different sintering conditions.

**Table 4.1** The relative densities under different SPS conditions

Changing Parameter	Sintering Conditions (°C-MPa-Min)	Relative Densities (%)
	900-60-5	99.2
	900-60-10	99.3
T:	900-60-20	98.9
Time	900-60-30	99.1
	900-60-45	99.0
	900-60-60	99.2
	600-60-5	99.3
	700-60-5	99.4
Temperature	800-60-5	99.2
	900-60-5	99.0
	1000-60-5	99.1

As shown, the relative densities were not affected significantly either by temperature or time. The XRD scans of time-varied samples are presented below. (**Figure 4.4**) The reference X-ray diffraction profile is needed for phase purity comparison; the PDF #043-1051 (single phase VO<sub>2</sub> profile) was used as a reference.

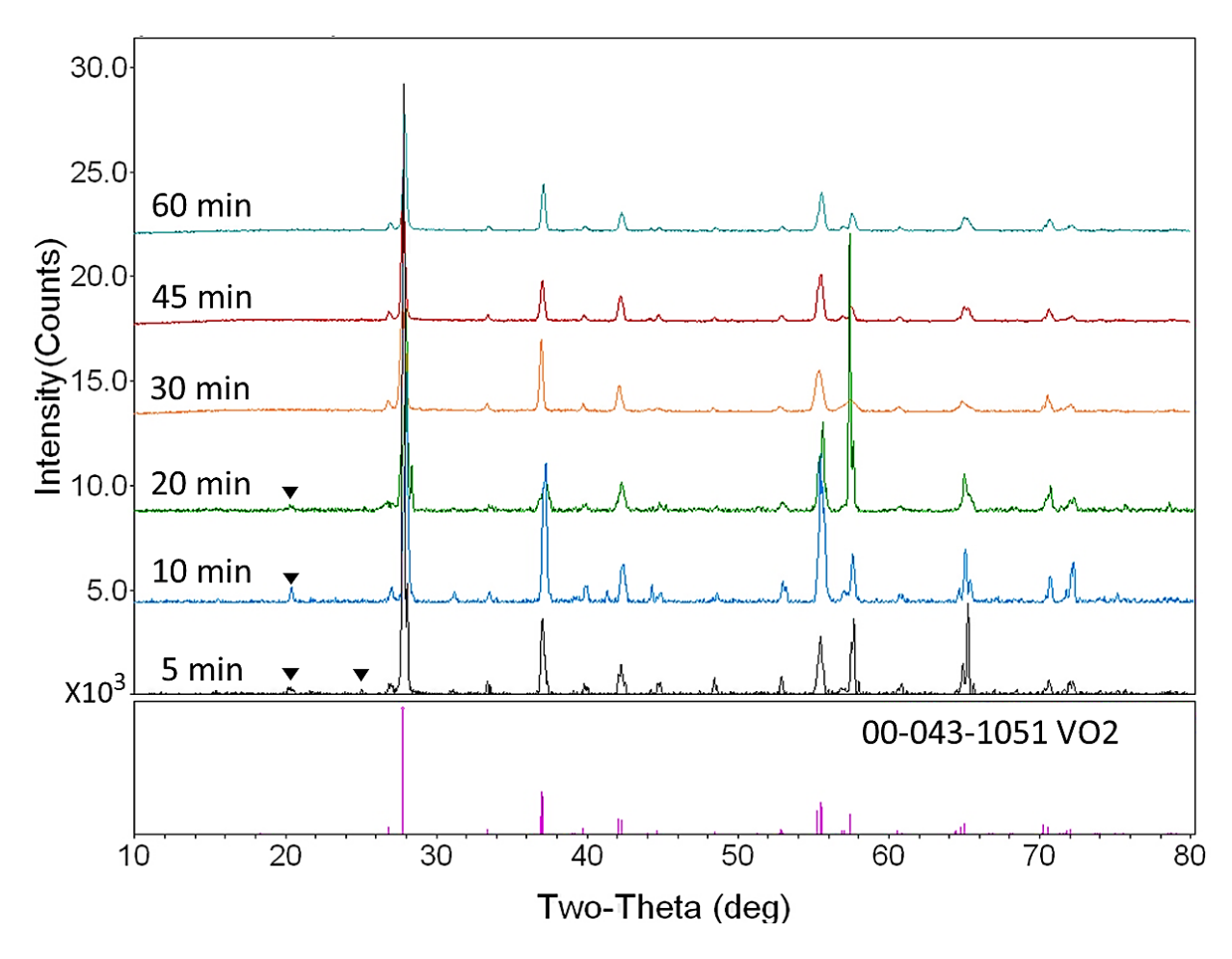


**Figure 4.4** The comparison of XRD scans of PECS time-varied samples (sintered for 5, 10, 20, 30, 45 and 60 minutes) to a pure VO<sub>2</sub> PDF

We found that as the time under which the sample is placed for sintering increased, the phase purity also increased. When the sintering time had reached 30 minutes, we obtained a single-phase VO₂. This can be observed if we focus on the impurity peak highlighted with ▼ mark on **Figure 4.4** above. It started disappearing as the sintering time increased, and the peak could not be seen anymore after 30-min sintering time. The reason is not clear but it could possibly be related to reducing atmosphere in SPS.

The effect of a sintering temperature was investigated as well. The following figure shows how varying temperature affects the final phase purity.

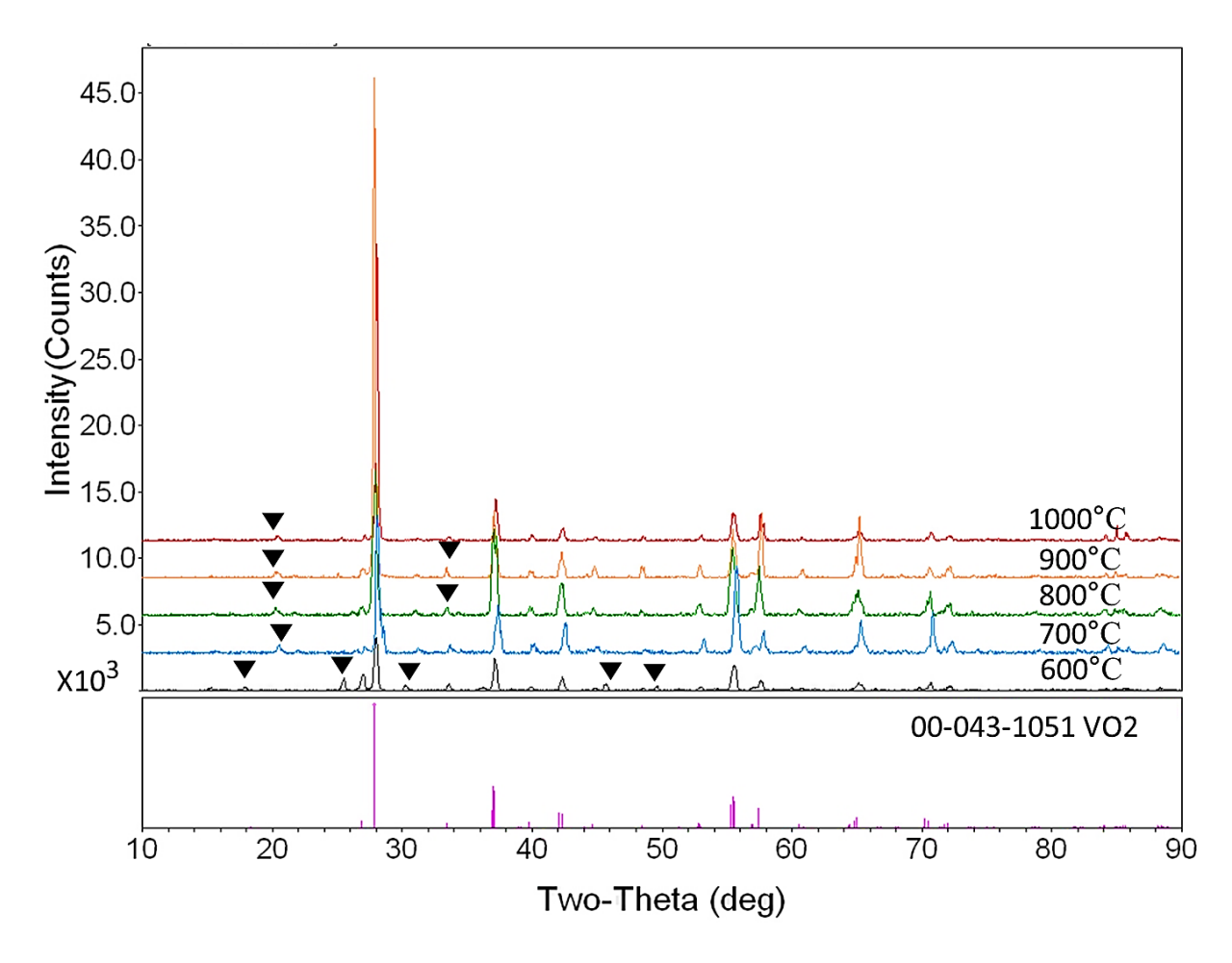


**Figure 4.5** The comparison of XRD scans of PECS temperature-varied samples (sintered at 600, 700, 800, 900 and 1000°C) to a pure VO<sub>2</sub> PDF. Samples were sintered for 5 minutes.

None of the samples yielded a perfect single-phase even at 1000°C as indicated by ▼ mark for impurity peaks in **Figure 4.5** although the highest-temperature sintered sample (1000°C-sample) showed the least number of impurity peaks. The impurity phases could not be identified.

Moreover, a higher temperature will produce a larger grain size which in turn will adversely affect  $k_{lat}$  in the insulating region. Thus, for further synthesis, a temperature of 900°C and a 30-minute sintering time would yield the best result.

The transport properties,  $\rho$  and k, of the single-phase VO<sub>2</sub> samples (900°C, 30, 45 and

60-minute, 60 MPa) were measured using the cryostat. The resistivity data is presented below. (**Figure 4.6**) As expected, the resistivity of the sample decreased drastically at the known IMT temperature, ~340K. The y-axis values were plotted in logarithmic scale. Note the logarithmic scale on the ordinate axis.

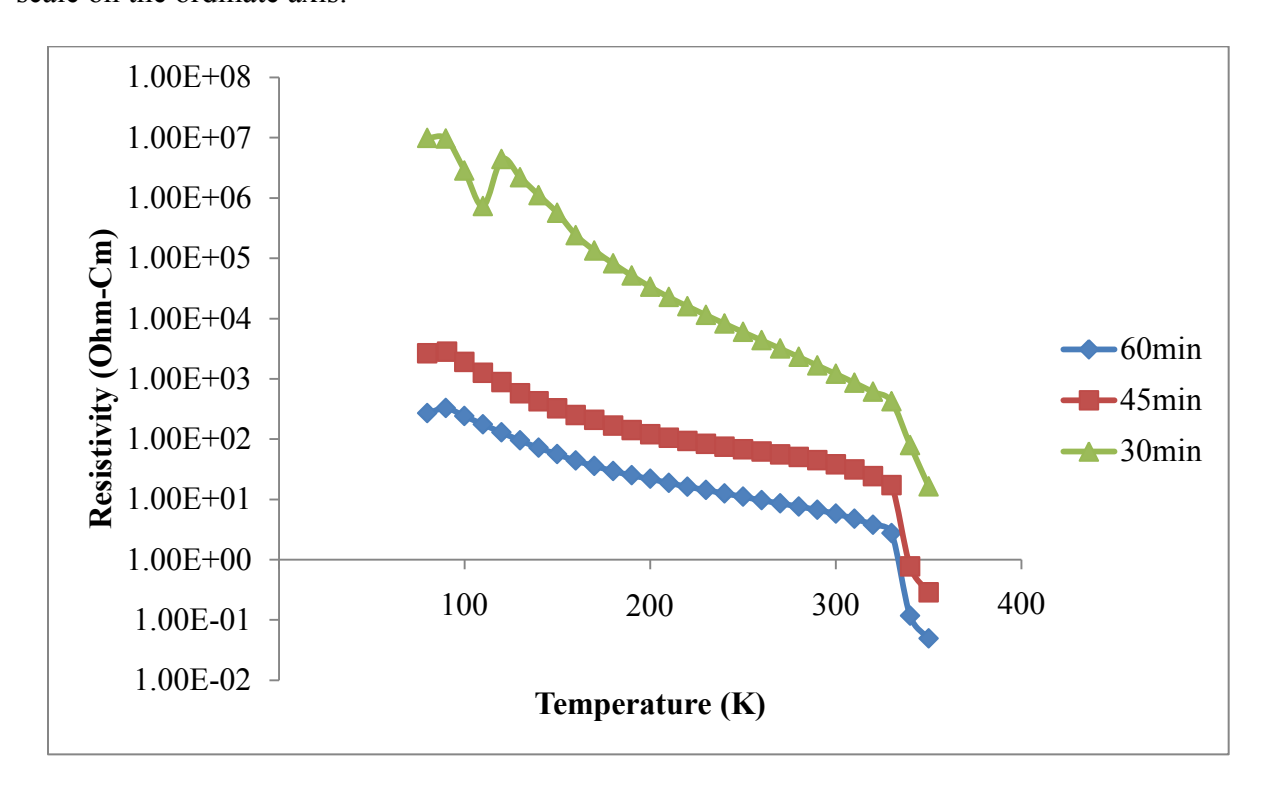


Figure 4.6 The resistivity of 30, 45 and 60-minute sintered samples

With increasing sintering time and temperature, the sample is subject to larger grain growth. With a larger grain size, there will be less grain-boundary scattering of electrons when they pass through the lattice. Thus, the lower resistivity in 60-minute sintered sample compared to the 30 or 45-minute ones seems reasonable. The 30-minute sintered sample has the highest resistivity,  $\rho$ .

The thermal conductivity data for these samples is presented below. (**Figure 4.7**) The k generally decreases with an increasing temperature except the 30-minute sintered sample which

showed a sudden jump at 200K.

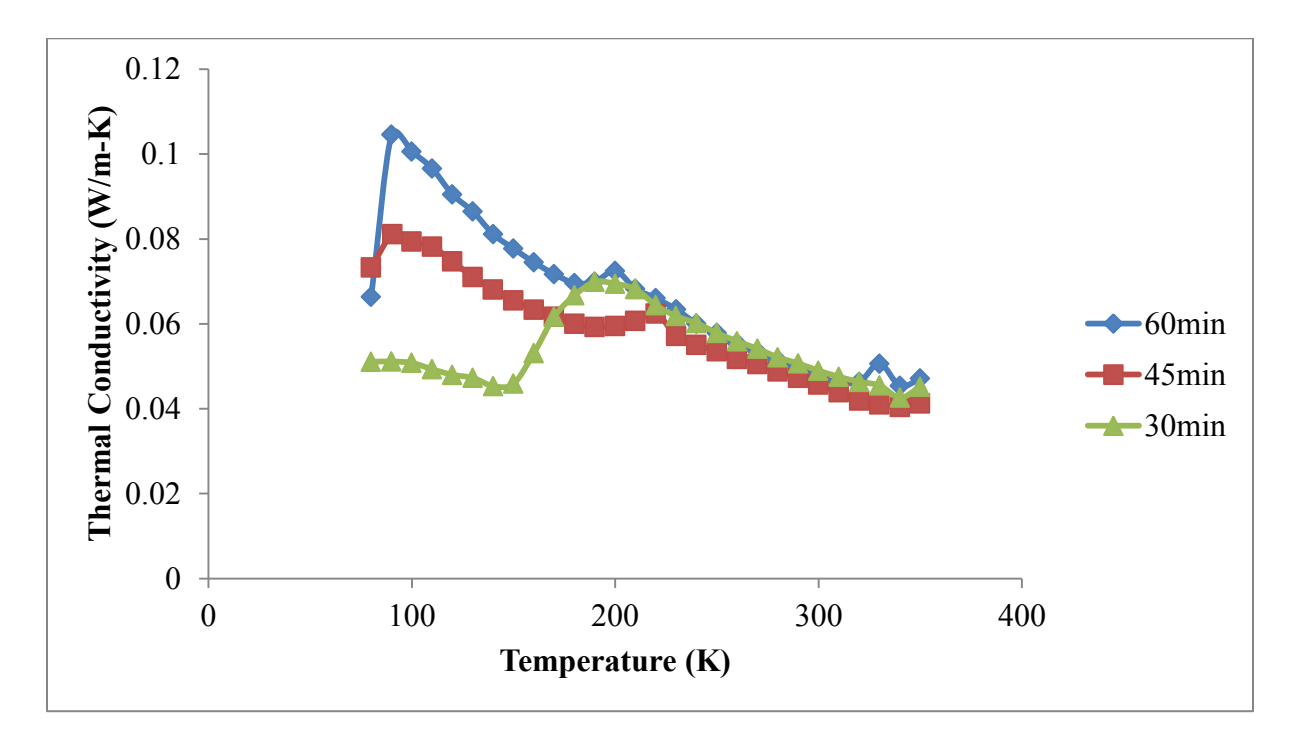


Figure 4.7 The thermal conductivity, k, of 30, 45 and 60-minute sintered samples.

This jump is abnormal since it is not the known IMT temperature for  $VO_2$ ; its origin is unknown and this sample was not studied further. Aside from this unusual behavior, it was seen clearly that more sintering time indeed led to increase of k. The obvious 'k jump' at IMT temperature was not observable, however. This result is congruent with the result Berglund obtained (**Figure 2.12**); Berglund claimed that he could not see a distinguishable change in k in a bulk  $VO_2$  sample even though he did not know a clear reason behind it.

The 60-minute sample was supposed to have the highest k due to the largest grain crystalline sizes. This was confirmed by our result although all the samples' k converged to almost the same level past 220K. Thus, we can conclude that the sintering time does not significantly affect the switching behavior.

### iii) Sol-Gel Technique Specimens

Other than using a commercially available VO<sub>2</sub>, our own synthesis of VO<sub>2</sub> powder was attempted by using a sol-gel technique. The sol-gel method is particularly useful because of its low-cost, ease of nano-particle formation and ability to dope with various metals. The basic principle of the sol-gel process is hydrolysis and condensation of precursors, typically metal alkoxides. [26, 27]

When a sol-gel technique-driven sample was obtained, the color of the sample looked different than SPS-driven ones. (**Figure 4.8**) It appeared 'greener' than the SPS sample (900°C, 60MPa, 30-minute sintered one selected for comparison).



Figure 4.8 The color difference between the samples obtained from (left) SPS (right) Sol-gel

The XRD result confirmed this difference; unlike the SPS sample, the sol-gel sample did not show a single-phase purity. (**Figure 4.9**) The impurity peaks (marked with **▼**) could not be identified. Thus, transport property measurement was not conducted.

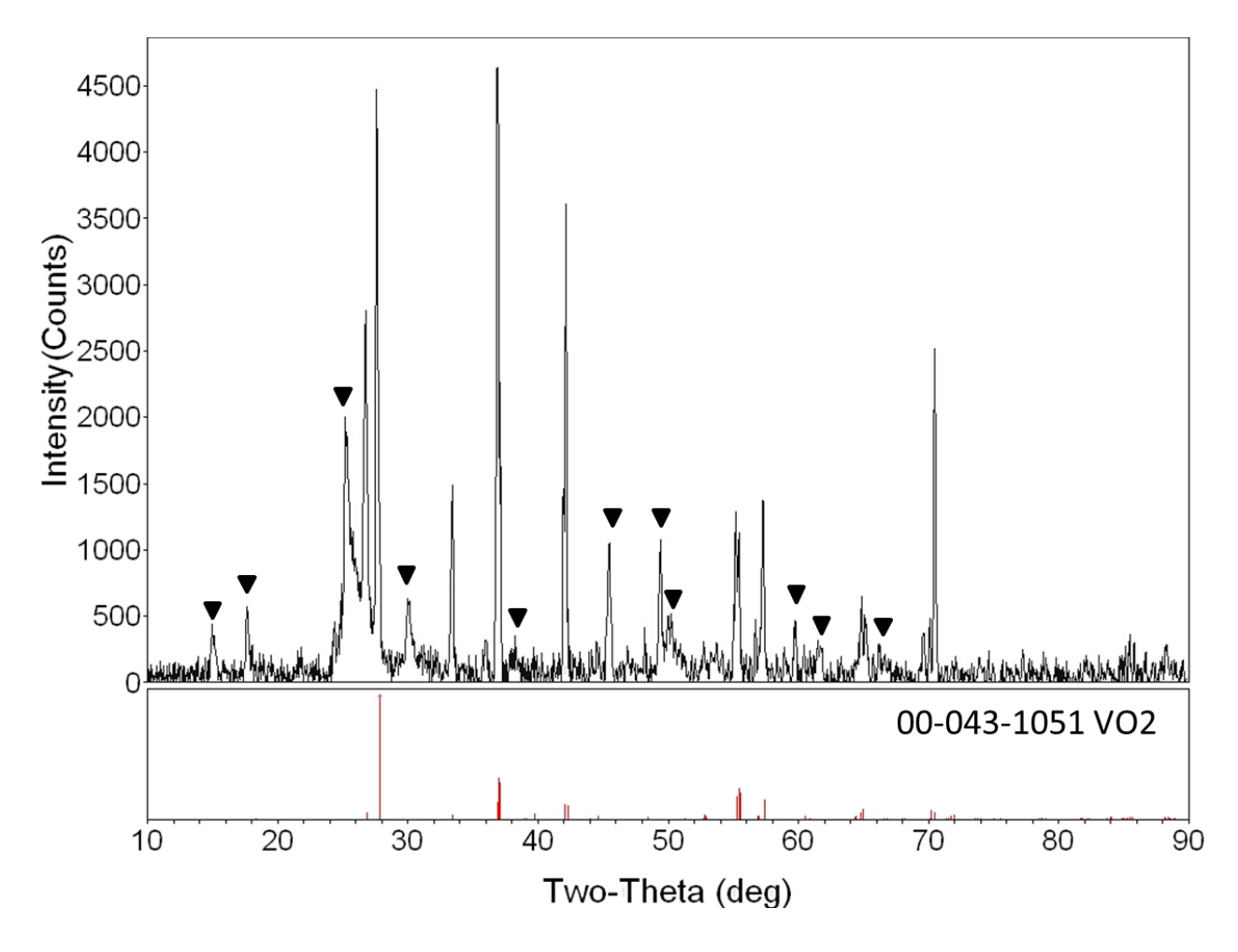
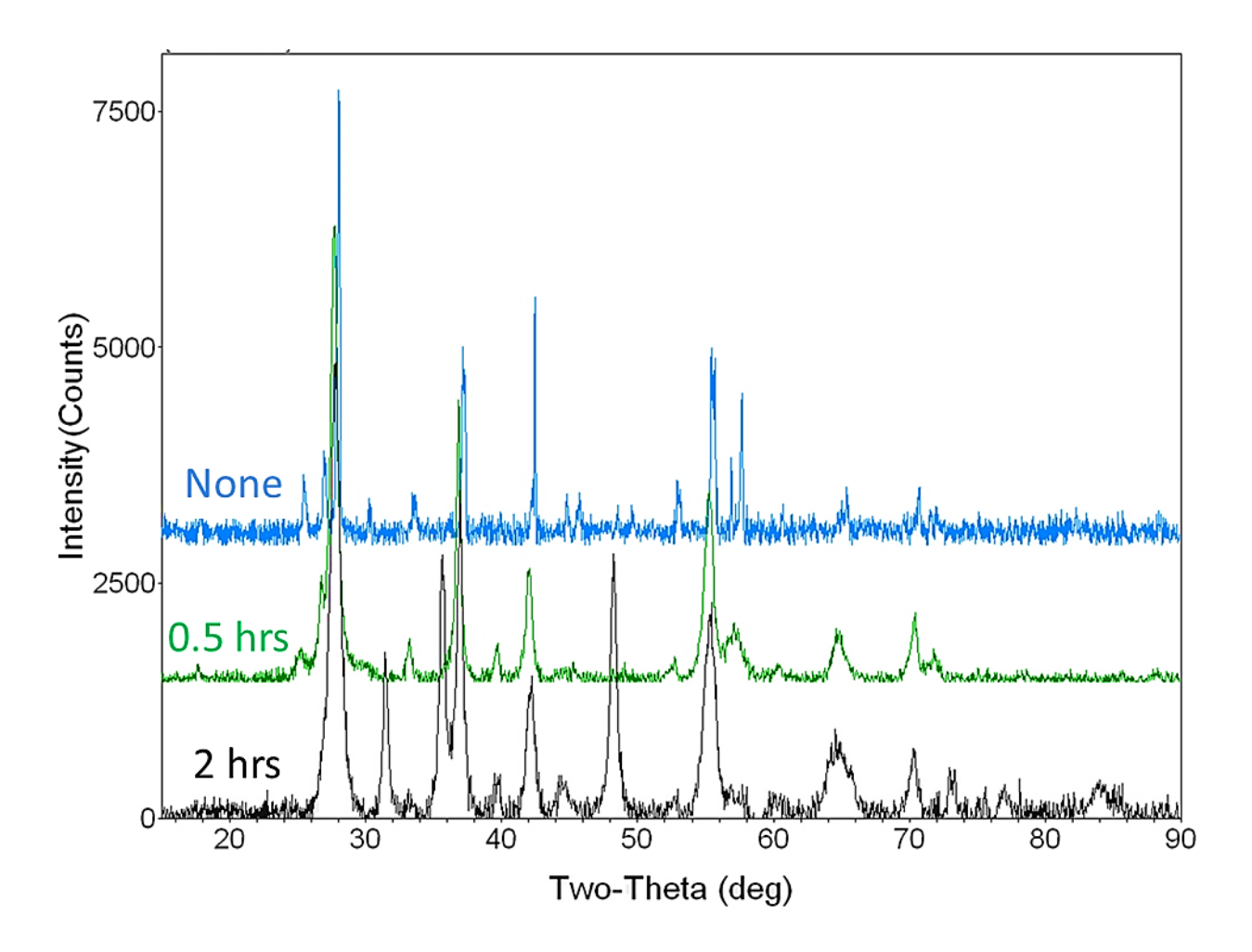


Figure 4.9 The XRD result of the sample obtained from sol-gel technique and the pure  $VO_2$  phase's PDF

# 4.2 Modifications on VO<sub>2</sub> specimens

### i) High-energy ball-milling

After ball milling the commercially available powder for a different amount of time, the XRD scans before sintering were conducted on each sample to see whether the ball milling indeed results in reduction in grain size. (**Figure 4.10**) As milling time increases, extra peaks appeared. This could be attributed to mechanical milling through high energy ball milling. Longer exposure to oxidation with longer milling could have also caused this.[28]



**Figure 4.10** The XRD scans of commercial VO<sub>2</sub> powder ball-milled for a different amount of time (none, 0.5 and 2 hours) before sintering

According to the Scherrer's equation, the FWHM (full-width at half maximum) values should widen as the crystalline sizes decrease. This relationship is shown in equation (4) below.

$$\tau = \frac{K\lambda}{\beta\cos\theta} \quad (4) [29]$$

where  $\tau$  is the mean size of the crystalline domains, K is a dimensionless shape factor (typically 0.9),  $\lambda$  is the X-ray wavelength,  $\beta$  is the FWHM in radians, and  $\theta$  is the Bragg angle.

Thus, larger grain sizes will induce narrower peaks while smaller grain sizes will induce

broader ones. However, this equation is mostly valid when the sample is nano-sized, and since we were not sure on our samples' particle sizes, the effect of ball-milling could only be observed in transport property measurement.

These samples were then subject to SPS under the same condition; sintering temperature, 900°C; sintering pressure, 60MPa and sintering time, 30 minutes. The obtained samples all showed densities above 99%. The XRD was conducted on them after sintering. (**Figure 4.11**)

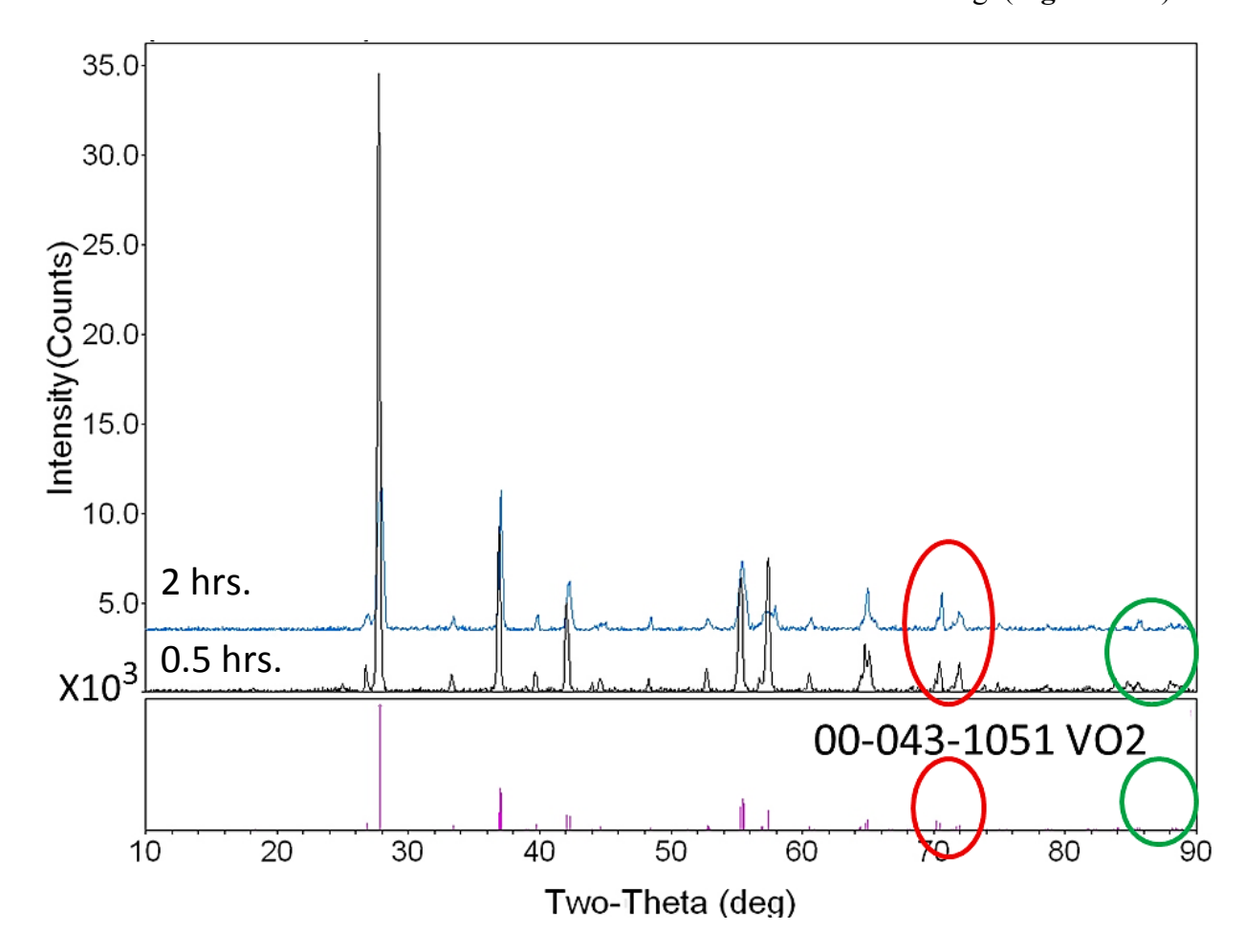


**Figure 4.11** The XRD result for differently ball-milled samples (0.5-hour and 2-hour milled) after sintering

One can see that sintering negated the effect of ball milling; almost no variations in FWHM could be found between two samples. It seems however that 2-hour milled sample

appeared less pure than the 30-minute milled sample. The circled areas in **Figure 4.11** show that the 30-minute milled sample (top curve) corresponds much closer to the available XRD PDF file than the 2-hour one (bottom curve). This could be due to a longer exposure to oxidation through ball-milling or more impurity phase produced from mechanical alloying.

However, because the difference was marginal and it still corresponds well to the given PDF file, we can confirm that 2-hour milled one is also composed of a single-phase  $VO_2$ . The transport properties were then measured for both samples. The k measurement result is presented below (**Figure 4.12**). The resistivity data were not obtained because ball-milling effect was intended to modify k only.

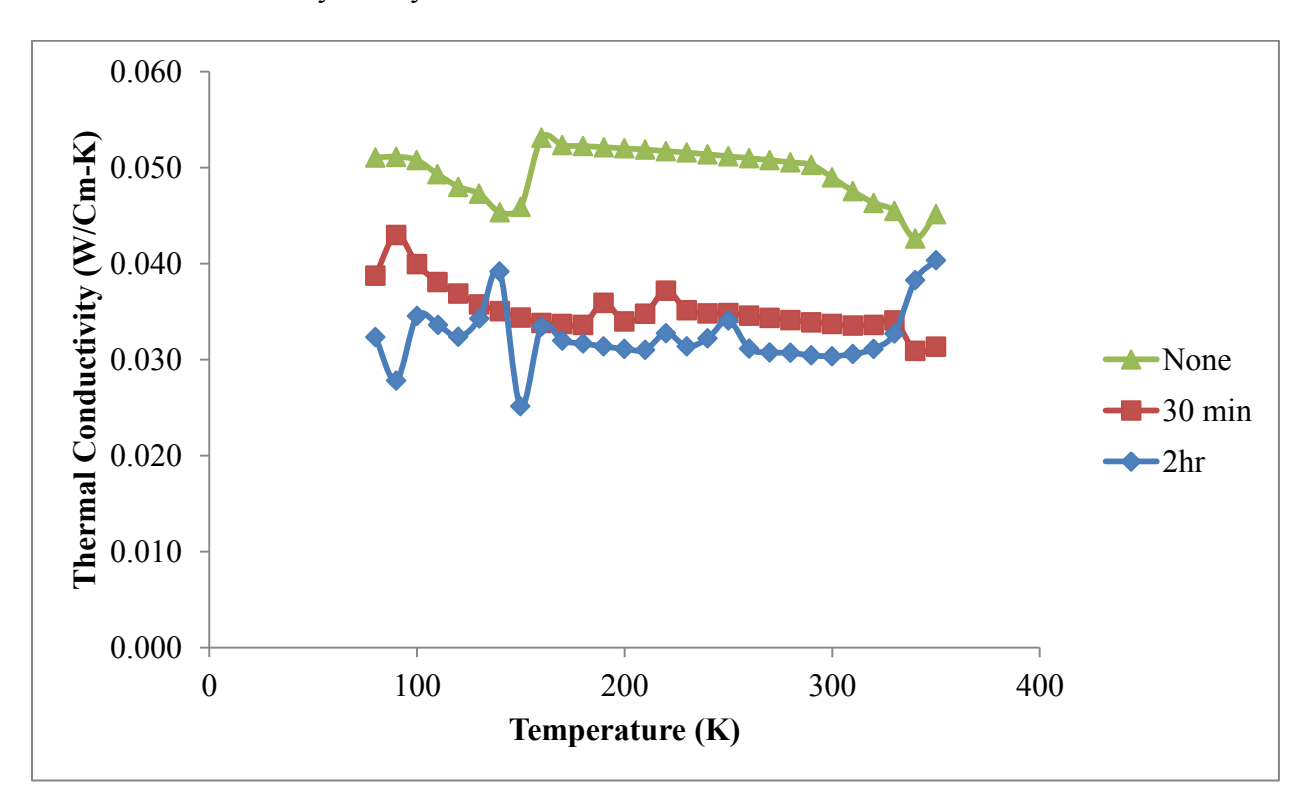


**Figure 4.12** The thermal conductivity, k, data comparison between differently ball-milled samples (none, 0.5 hours, 2 hours)

From equation (3), one can see that reduction of  $k_{lat}$ . should be witnessed when the phonon mean free path, l, is reduced. Thus, longer ball-milling is supposed to suppress  $k_{lat}$ . more than shorter milling. This phenomenon was observed as presented in Figure 4.12 above where the 2 hour milled sample showed the lowest k below the transition temperature while the non-milled one showed the highest result.

Although the 2 hour-milled sample showed the lowest k as intended, the difference between 30-min milled one and the 2 hour-milled one was marginal. Therefore, 30-min milling should be enough for reduction in k.

The 2 hour milled sample showed the highest switching in k through IMT even though this effect was not expected. Even though this result is meaningful, we cannot entirely trust it because the XRD result revealed we do not have a pure single-phase VO<sub>2</sub> in a 2-hour milled sample.

# ii) VO<sub>2</sub>-Cu Composites

The amount of Cu added to the VO<sub>2</sub> system ranges from 2at% to 5at%. The XRD scan result for each sample before sintering is presented below. (**Figure 4.13**) The peaks marked with  $\bigstar$  were identified as those belong to Blossite structure, and those marked with  $\blacktriangledown$  could not be identified.

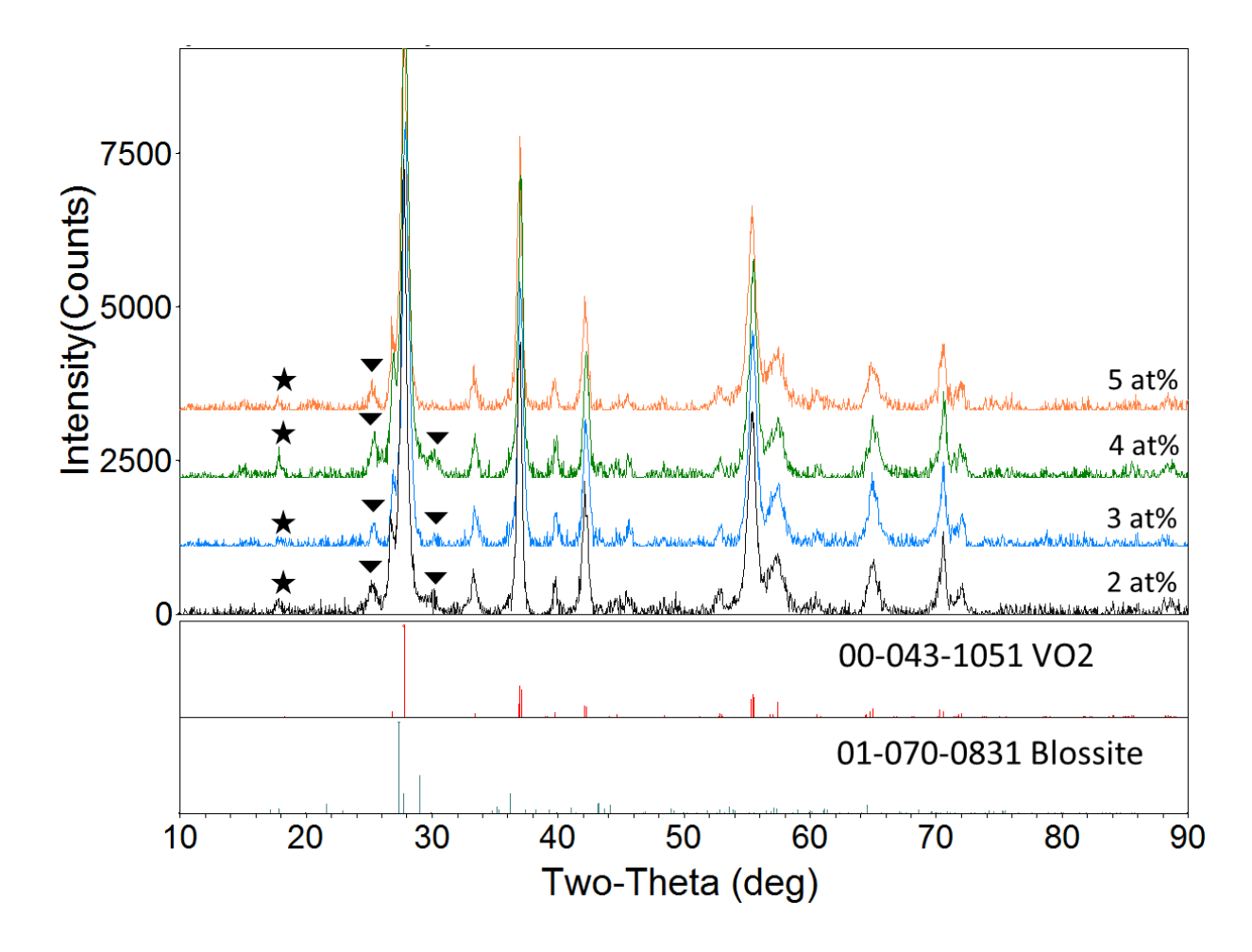


**Figure 4.13** The XRD results of different VO<sub>2</sub>-Cu composites (Cu 2 at%, 3 at%, 4 at%, 5 at%) before sintering with a comparison to available PDFs of pure VO<sub>2</sub> and Blossite structure

Even though the amount of Cu added to the system increased, the XRD result did not reveal clear difference between each sample. According to XRD result, the samples could take on 'blossite' structure, Cu<sub>2</sub>V<sub>2</sub>O<sub>7</sub>. However, the result was much closer to the pure VO<sub>2</sub> PDF. Clear presence of Cu or Cu-oxides were not observed either.

The SPS was conducted on each sample. The SPS condition was held the same for each sample at a temperature of 900 °C, pressure of 60MPa, and a holding time of 30 minutes. The XRD was conducted for each sample after sintering. (**Figure 4.14**) The obtained samples all

showed densities above 99%.

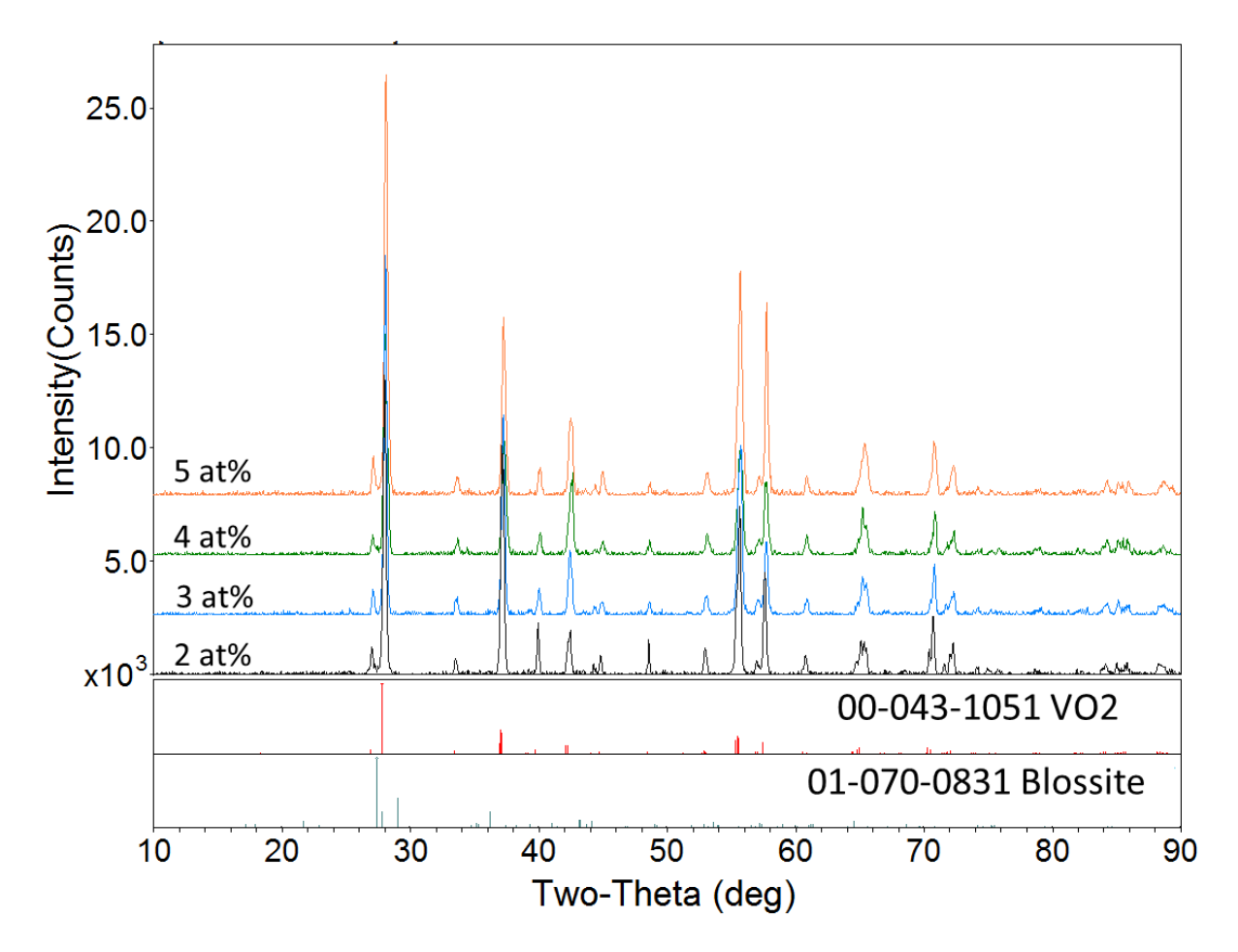


**Figure 4.14** The XRD results of different VO<sub>2</sub>-Cu composites (Cu 2 at%, 3 at%, 4 at%, 5 at%) after sintering with a comparison to available PDFs of pure VO<sub>2</sub> and Blossite structure

Similar to before-sintering case, the XRD results match almost perfectly to pure  $VO_2$  regardless of Cu content. The blossite structure was the most possible candidate accounting for Cu addition. The impurity peaks could not be identified.

The transport properties,  $\rho$  and k, were measured for each sample. The result is presented below. (**Figure 4.15**) It is assumed that with Cu addition, the resistivity should decrease. It was actually confirmed in the result because the pure sample (non-Cu added) showed much higher resistivity than the Cu-added ones.

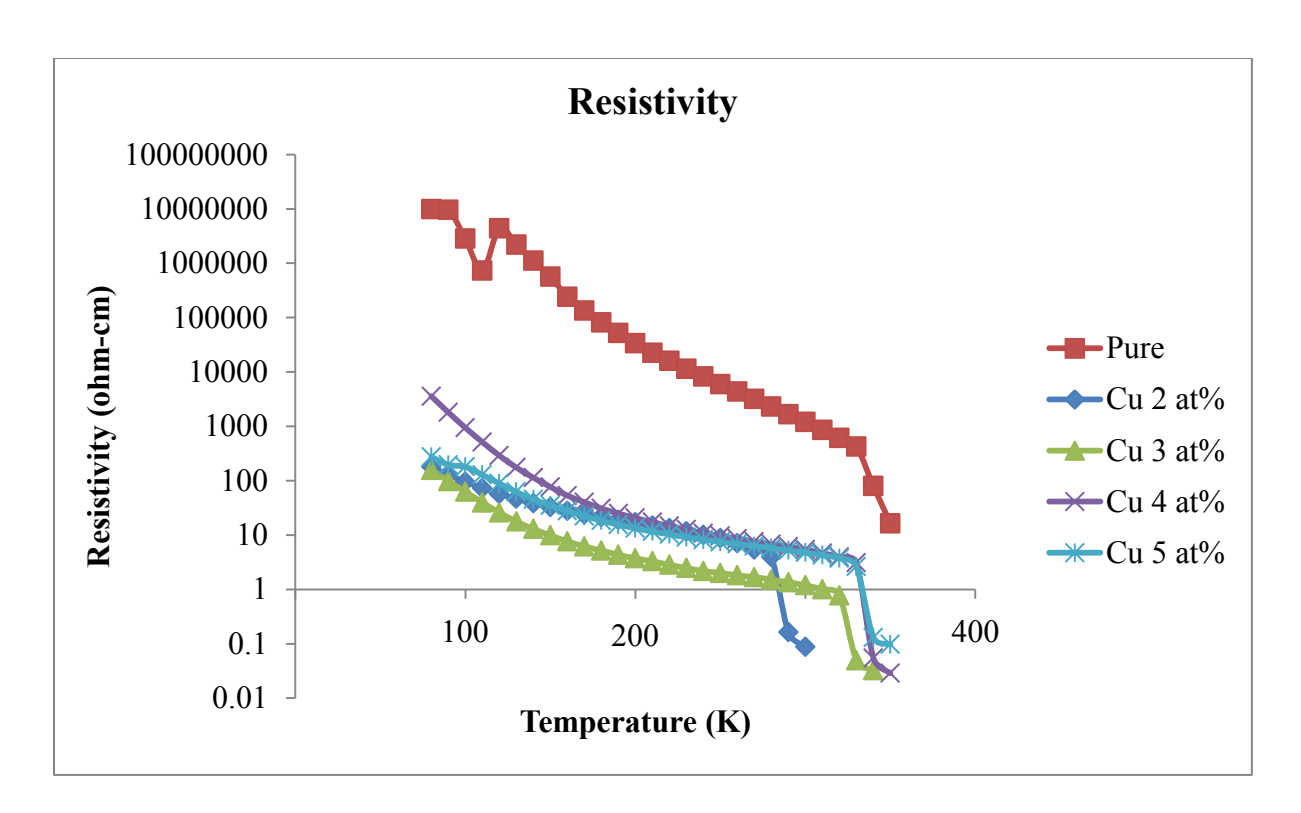


Figure 4.15 The resistivity, **ρ**, of various Cu-added samples (Cu 2 at%, 3 at%, 4 at%, 5at%)

However, more Cu addition did not lead to more reduction of resistivity in our experiment. The lowest resistivity was observed in the Cu 3 at% sample while the highest was observed in Cu 4 at% although the difference was not large. Also, the Cu 5 at% sample had a higher resistivity than Cu 3 at% one.

When these results were compared to the literature data shown in **Figure 2.15**, they matched quite well although ours showed generally higher  $\rho$  than the literature sample. The reason could be attributed their samples containing not only VO<sub>2</sub>, but also 15 wt% VPG as a default composition.

One interesting phenomenon is the transition in a Cu 2 at% sample. As seen in Figure 4.16, the Cu 2 at% sample showed a transition approximately at 280K. This is significantly lower than the other samples' or a known transition temperature of 340K. It indicates that we obtained

a different material or phase than others. This phenomenon is also observable for Cu 3 at% sample as well where the transition occurred slightly below 350K (around 325K). This could be attributed to an unexpectedly low resistivity of the Cu 3 at% sample. However, XRD results shown in Figure 4.14 did not reveal a significant difference among samples. This disorder might have happened due to loss of Cu particles during sintering.

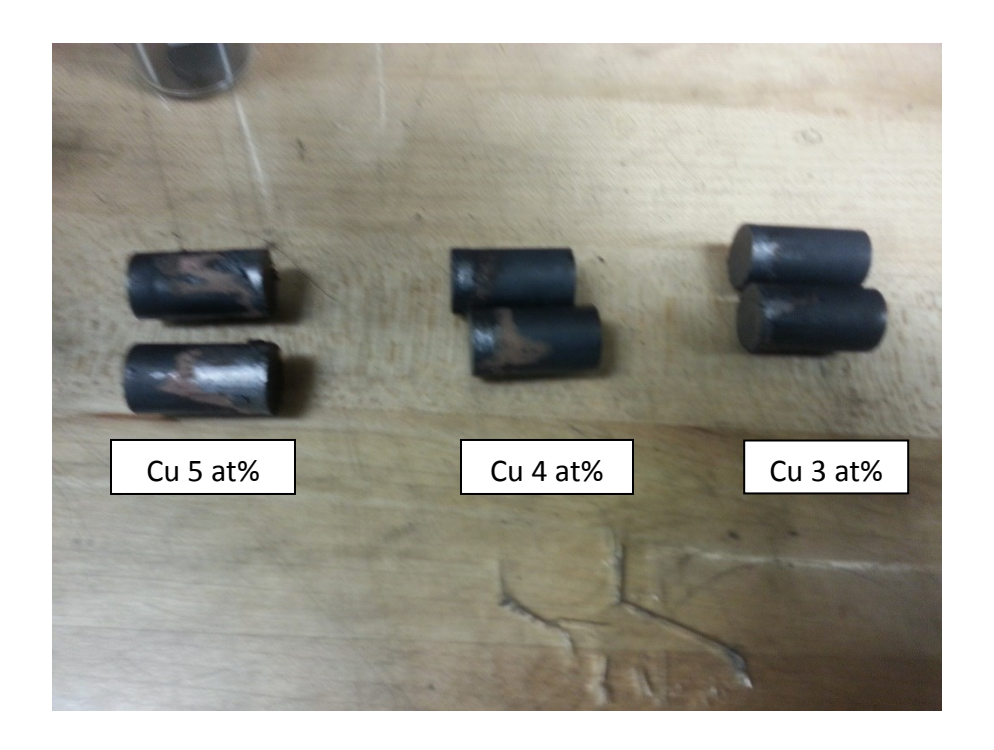


**Figure 4.16** The pictures of graphite die punches used in SPS for 3 at%, 4 at%, and 5 at% VO<sub>2</sub>-Cu composites

As seen in **Figure 4.16**, with more Cu content added to the system, we could observe more of 'red, Cu-colored' areas on the graphite die punches. This means more Cu leaked out of the die during sintering (Cu loss). In the figure, we can see Cu 5 at% sample shows the most loss of Cu, and the least in 3 at%. This is the most probable reason why Cu 3 at% sample showed the lowest resistivity in **Figure 4.15**.

The change in k was observed but to a much lesser extent than expected. (Figure 4.17) The Cu 4 at% sample showed the highest k. It was even higher than the Cu 5at % one which is counter-intuitive. This could be attributed to the more Cu loss in the 5 at% sample during sintering. The Cu 2 at% sample was excluded for further analysis on an assumption that it is composed of very different phases or materials. This was merely an assumption because the XRD result did not show any discrepancies when compared to the pure VO<sub>2</sub> PDF as seen in

**Figure 4.14**.

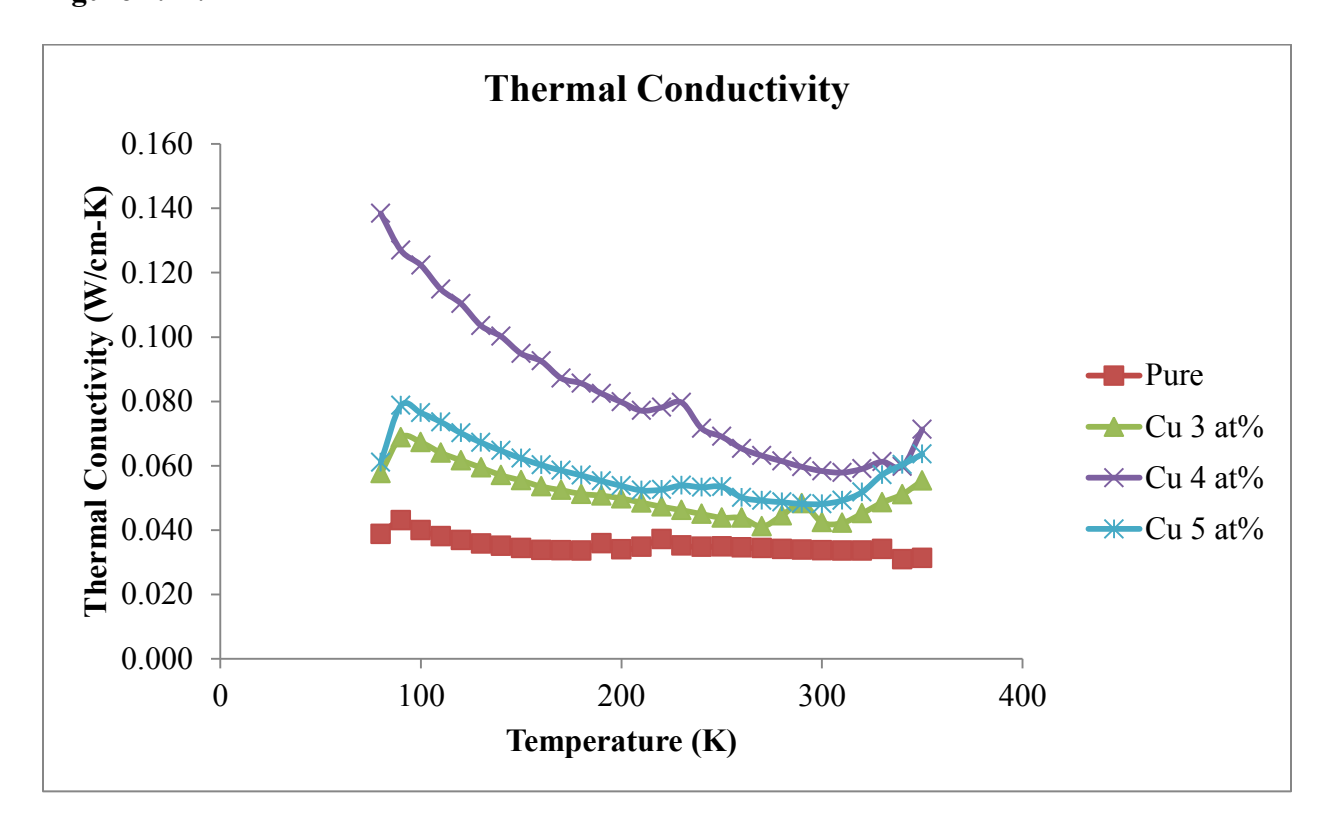
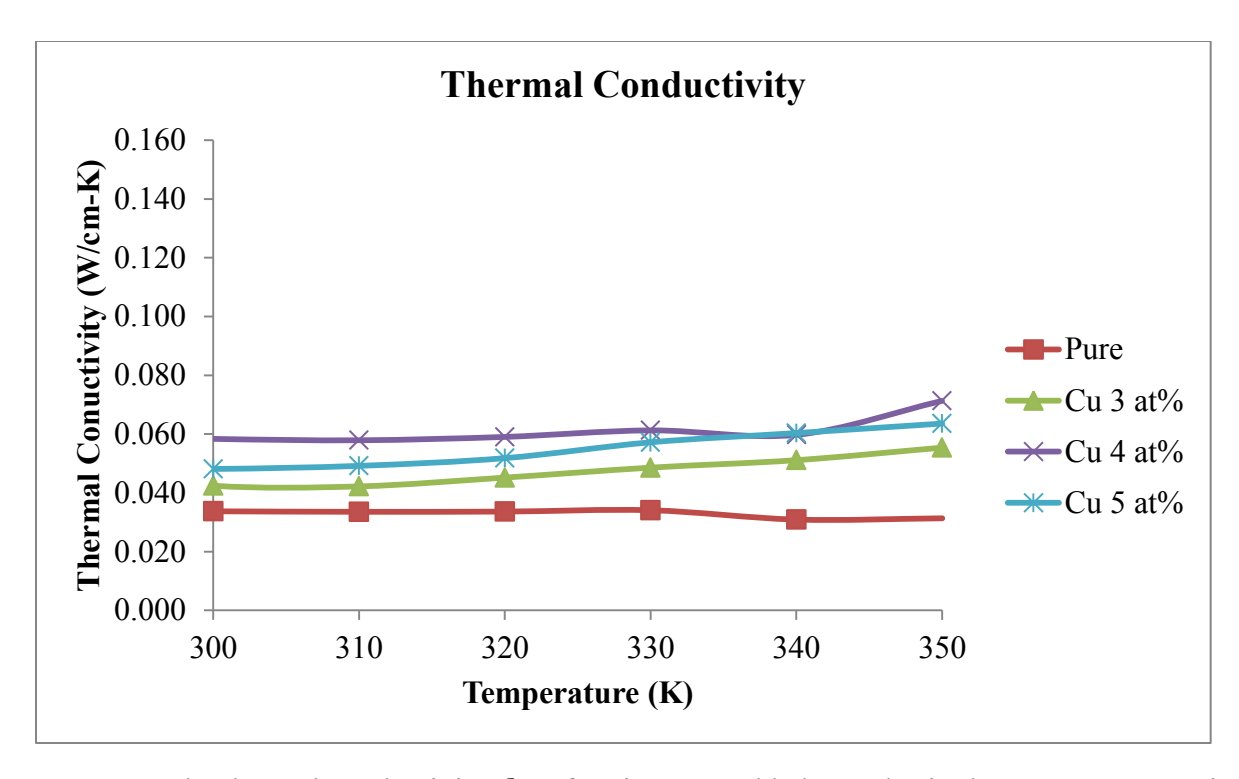


Figure 4.17 The thermal conductivity, k, of the Cu-VO<sub>2</sub> composite samples in the whole temperature region (80K-350K)

For better comparison of the jump in k, only the region near the known transition temperature was plotted. Such region ranges from 300K to 350K. (**Figure 4.18**)



**Figure 4.18** The thermal conductivity, k, of various Cu-added samples in the 300K-350K region

The comparison result is tabulated below. (**Table 4.2**) It was discovered that Cu 5 at%-added sample showed the highest change in k while the lowest change was seen in the pure sample. This was the expected result. However, considering the previous observation of the most Cu loss in the 5% system, it cannot be taken as firm evidence of the influence of Cu. Thus, other than the Cu loss, the non-uniformity could be a reason. Non-uniformity is not desirable because only part of the system will experience enhancement in k.

**Table 4.2** The **k** changes in a 300K-350K region for different VO<sub>2</sub>-Cu composites

Sample	<b>k</b> minima	<b>k</b> maxima	% change in <b>k</b>
	(W/cm-K)	(W/cm-K)	(%)
Pure	0.0309	0.0313	1.278
Cu 3 at%	0.0420	0.0550	30.95
Cu 4 at%	0.0580	0.0710	22.41
Cu 5 at%	0.0480	0.0640	33.33

If scanning electron microscopy (SEM) or energy dispersive X-ray spectroscopy (EDS) is conducted, we could see how Cu particles are distributed in the matrix and thus be able to explain better why we get higher or lower change in k.

Moreover, in **Figure 4.17**, we can find that the  $\kappa$  still shows an upward trend at 350K, the maximum reachable temperature in the Cryostat machine. Thus, if we conduct a higher temperature measurement, we might be able to see more increase in k at a higher temperature region.

#### **CHAPTER 5. Conclusions**

To achieve optimal performance of VO<sub>2</sub>-based thermal switches, the thermal conductivity transition should be made much more distinguishable through IMT. This issue could be addressed with decreasing grain size to lower the lattice thermal conductivity at low temperatures while using a VO<sub>2</sub>-metal composite material to increase the electronic thermal conductivity at high temperatures.

First, synthesizing high purity VO<sub>2</sub> bulk samples is crucial. Among various methods, spark plasma sintering turned out to be the most effective. Although higher temperature and longer sintering time helps yield a higher purity sample, those parameters will entail large grain growth, which is adverse for thermal conductivity reduction. Thus, a sintering temperature of 900°C and time of 30 minutes were chosen as a compromise.

For the reduction of lattice thermal conductivity, grain size reduction technique such as ball-milling was used. It was found that longer ball-milling time leads to a reduction in thermal conductivity at lower temperatures as expected. The 2-hour ball-milled sample even showed a better switching behavior although whether this could be reproduced is questionable.

For the enhancement of electronic thermal conductivity, a composite concept was adopted. A composite of VO<sub>2</sub> matrix and highly conductive metal inclusions such as Cu should give us increase in electronic thermal conductivity after IMT. It was determined that Cu addition was beneficial for better thermal switching. However, the loss of Cu during sintering should be taken care of for accurate stoichiometry control. In this experiment, the sample with the highest Cu concentration showed the best switching behavior as expected.

## **CHAPTER 6. FUTURE RESEARCH CONSIDERATIONS**

Thermal switches are innovative in a sense that they can control temperatures at a setvalue without requiring additional components or power sources. A better thermal switching behavior will be achieved if the degree of switching is enhanced greatly.

Therefore, in VO<sub>2</sub> system where it is an insulator at a lower temperature and a metal at a higher temperature, substantial decrease in  $k_{lat}$  and increase in  $k_{elec}$  will be required.

For more reduction of  $k_{lat}$ , a grain growth inhibitor can be used other than ball-milling. Such inhibitors, for example, can be  $ZrO_2$  or  $Al_2O_3$ . These materials are known to inhibit grain growth during sintering.[30, 31]

Also, organic agent such as oleic acid, OA, is also known to prevent grain agglomeration during ball-milling. Thus, the addition of OA during ball-milling could be beneficial for lower  $k_{lat}$ . [32]

The  $k_{elec}$  can be enhanced more if we use higher thermally conducting materials as inclusions. The example of the materials having a higher thermal conductivity than copper includes silver or carbon nanotubes.

The mechanical properties of bulk VO<sub>2</sub> need to be improved substantially because all the bulk samples obtained in this work were too brittle. This will inhibit a wide industrial use. In addition, finding other IMT materials having better switching behavior and lower cost is also required.

BIBLIOGRAPHY

#### **BIBLIOGRAPHY**

- 1. Bardeen, J. and W.H. Brattain, *The transistor, a semi-conductor triode*. Physical Review, 1948. 74(2): p. 230.
- 2. Perlin, P., et al., *Metal-Insulator Transition in GaN Crystals*. physica status solidi (b), 1996. 198(1): p. 223-233.
- 3. Whitten, K.W., *Chemistry*. 2014, Belmont, CA: Brooks/Cole Cengage Learning.
- 4. Serway, R.A.J.J.W., *Physics for scientists and engineers. Volume 5, Volume 5.* 2010, Pacific Grove, Calif.; Andover: Brooks/Cole; Cengage Learning [distributor].
- 5. Zhang, R.-z., et al., *Thermoelectric transport coefficients of n-doped CaTiO3, SrTiO3 and BaTiO3: A theoretical study.* Physica B: Condensed Matter, 2012. 407(7): p. 1114-1118.
- 6. Chandra, S., *Comprehensive inorganic chemistry (for B.Sc 1st year)*. 2004, New Delhi, India: New Age International (P) Ltd. Pub.
- 7. Nag, J. and R. Haglund Jr, *Synthesis of vanadium dioxide thin films and nanoparticles*. Journal of Physics: Condensed Matter, 2008. 20(26): p. 264016.
- 8. Maaza, M., et al., *Direct production of thermochromic VO2 thin film coatings by pulsed laser ablation.* Optical Materials, 2000. 15(1): p. 41-45.
- 9. Si, C., et al., *Metal-insulator transition in V(1-x)W(x)O2: structural and electronic origin.* Phys Chem Chem Phys, 2012. 14(43): p. 15021-8.
- 10. Yang, Z., C. Ko, and S. Ramanathan, *Oxide electronics utilizing ultrafast metal-insulator transitions*. Annual Review of Materials Research, 2011. 41: p. 337-367.
- 11. Zhou, Y. and S. Ramanathan, *Correlated Electron Materials and Field Effect Transistors for Logic: A Review.* arXiv preprint arXiv:1212.2684, 2012.
- 12. Dorokhov, O.N., *On the coexistence of localized and extended electronic states in the metallic phase.* Solid State Communications, 1984. 51(6): p. 381-384.
- 13. Kim, H.T., et al., Abrupt metal-insulator transition device, circuit for removing high-voltage noise using the abrupt metal-insulator transition device, and electrical and/or electronic system comprising the circuit, 2009, European Patent # EP 1911137 A1
- 14. Yong, Z., et al., *Electrically controlled metal–insulator transition process in VO 2 thin films*. Journal of Physics: Condensed Matter, 2012. 24(3): p. 035601.

- 15. Feng, X.M., X.P. Ai, and H.X. Yang, *A positive-temperature-coefficient electrode with thermal cut-off mechanism for use in rechargeable lithium batteries*. Electrochemistry Communications, 2004. 6(10): p. 1021-1024.
- 16. Bush, C.H., *Thermal switch for battery protection*, 1991,U.S Patnet # US5070427.
- 17. Gilmore, D.G., *Spacecraft thermal control handbook Vol. 1 Vol. 1.* 2002, El Segundo, Calif: Aerospace Press [u.a.].
- 18. Ho, C.Y., et al., *Thermal conductivity of ten selected binary alloy systems*. Journal of Physical and Chemical Reference Data, 1978. 7(3): p. 959-1178.
- 19. Griffiths, C.H. and H.K. Eastwood, *Influence of stoichiometry on the metal-semiconductor transition in vanadium dioxide*. Journal of Applied Physics, 1974. 45(5): p. 2201-2206.
- 20. Li, Y., et al., Core-shell VO2@TiO2 nanorods that combine thermochromic and photocatalytic properties for application as energy-saving smart coatings. Sci Rep, 2013. 3: p. 1370.
- 21. Zhang, Y. and S. Ramanathan, *Analysis of "on" and "off" times for thermally driven VO2 metal-insulator transition nanoscale switching devices.* Solid-State Electronics, 2011. 62(1): p. 161-164.
- 22. Berglund, C. and H. Guggenheim, *Electronic Properties of VO\_{2} near the Semiconductor-Metal Transition*. Physical Review, 1969. 185(3): p. 1022.
- 23. Oh, D.-W., et al., Thermal conductivity and dynamic heat capacity across the metal-insulator transition in thin film< equation>< font face='verdana'> VO</font>< sub> 2</sub></equation>. Applied Physics Letters, 2010. 96(15): p. 151906-151906-3.
- 24. Kolbunov, V., A. Ivon, and I. Chernenko, *Influence of a high conductivity additive on the electrical properties of vanadium dioxide-based ceramics*. Journal of the European Ceramic Society, 2003. 23(9): p. 1435-1439.
- 25. O'Brien, R.C., et al., *Spark Plasma Sintering of simulated radioisotope materials within tungsten cermets.* Journal of Nuclear Materials, 2009. 393(1): p. 108-113.
- 26. Siciliano, P., *Preparation, characterisation and applications of thin films for gas sensors prepared by cheap chemical method.* Sensors and Actuators B: Chemical, 2000. 70(1–3): p. 153-164.
- 27. Brinker, C.J.S.G.W., *Sol gel science : the physics and chemistry of sol-gel processing*. 1993, Boston [u.a.]: Acad. Press.

- 28. Calka, A. and A.P. Radlinski, *Universal high performance ball-milling device and its application for mechanical alloying*. Materials Science and Engineering: A, 1991. 134(0): p. 1350-1353.
- 29. Monshi, A., *Modified Scherrer Equation to Estimate More Accurately Nano-Crystallite Size Using XRD*. World Journal of Nano Science and Engineering, 2012. 02(03): p. 154-160.
- 30. Fisher, J.G., et al., *Inhibition of abnormal grain growth in BaTiO3 by addition of Al2O3*. Journal of the European Ceramic Society, 2006. 26(9): p. 1619-1628.
- 31. Lange, F.F. and M.M. Hirlinger, *Hindrance of Grain Growth in Al2O3 by ZrO2 Inclusions*. Journal of the American Ceramic Society, 1984. 67(3): p. 164-168.
- 32. Zhang, Q., et al., Suppression of grain growth by additive in nanostructured p-type bismuth antimony tellurides. Nano Energy, 2012. 1(1): p. 183-189.
- 33. Electronics and Telecommunications Research Institute (ETRI), South Korea, "Report Data for Media (2006-76) / ETRI, MIT 원리 적용 임계온도 스위치 개발성공 휴대폰, 노트북 배터리 부풀림 및 폭발방지 적용가능" (ETRI, MIT mechansim applied-ciritcal temperature thremal switch devleopment success Applications in cell phone, laptop battery swell and explosion prevention). The Korean version can be obtained at "http://www.etri.re.kr/etri/pro/pro\_01010000.etri?type=view&b\_idx=2182"
- 34. A&D Company Limited, *GX-13 Density Determination Kit For GX-200/400/600 Instruction Manual*, can be obtained at www.aandd.jp/products/manual/balances/gx-13.pdf
- 35. S.M Marcus and R.L. Blaine, *Thermal Conductivity of Polymers, Glasses & Ceramics by Modulated DSC*, Thermochimica Acta 243.2 (1994): 231-239
- 36. Griffith C H and Eastwood H K 1974 Influence of stoichiometry on metal.semiconductor transition in vanadium dioxide J. Appl. Phys. 45 2201.6